The American Journal of Pathology, Vol. 193, No. 4, April 2023

ELSEVIER

The American Journal of
PATHOLOGY

ajp.amjpathol.org

TUMORIGENESIS AND NEOPLASTIC PROGRESSION

SMARCB1 Loss in Poorly Differentiated Chordomas Drives Tumor Progression

Tara A. Walhart,* Bryanna Vacca,*† Austin J. Hepperla,* Samera H. Hamad,*† James Petrongelli,* Yemin Wang,‡§ Erin L. McKean,¶ Michelle Moksa,‖** Qi Cao,‖** Stephen Yip,‡§ Martin Hirst,‖** and Bernard E. Weissman*†,††

From the Lineberger Comprehensive Cancer Center, Curriculum in Toxicology and Environmental Medicine,† and the Department of Pathology and Laboratory Medicine,†† University of North Carolina at Chapel Hill School of Medicine, Chapel Hill, North Carolina; the Departments of Pathology and Laboratory Medicine‡ and Microbiology & Immunology,‖ Michael Smith Laboratories, University of British Columbia, Vancouver, British Columbia, Canada; the Department of Molecular Oncology,§ British Columbia Cancer Research Institute, Vancouver, British Columbia, Canada; the Department of Otolaryngology and Neurosurgery,¶ University of Michigan, Ann Arbor, Michigan; and Canada's Michael Smith Genome Sciences Centre at BC Cancer,** Vancouver, British Columbia, Canada*

Accepted for publication December 20, 2022.

Address correspondence to Bernard E. Weissman, Ph.D., Lineberger Comprehensive Cancer Center, University of North Carolina, 450 West Dr., Room 31-322, Chapel Hill, NC 27599-7295.
E-mail: weissman@med.unc.edu.

Poorly differentiated (PD) chordoma, a rare, aggressive tumor originating from notochordal tissue, shows loss of SMARCB1 expression, a core component of the Switch/Sucrose Non-Fermentable (SWI/SNF) chromatin remodeling complexes. To determine the impact of SMARCB1 re-expression on cell growth and gene expression, two SMARCB1-negative PD chordoma cell lines with an inducible SMARCB1 expression system were generated. After 72 hours of induction of SMARCB1, both SMARCB1-negative PD chordoma cell lines continued to proliferate. This result contrasted with those observed with SMARCB1-negative rhabdoid cell lines in which SMARCB1 re-expression caused the rapid inhibition of growth. We found that the lack of growth inhibition may arise from the loss of CDKN2A ($p16^{INK4A}$) expression in PD chordoma cell lines. RNA-sequencing of cell lines after SMARCB1 re-expression showed a down-regulation for rRNA and RNA processing as well as metabolic processing and increased expression of genes involved in cell adhesion, cell migration, and development. Taken together, these data establish that SMARCB1 re-expression in PD chordomas alters the repertoire of SWI/SNF complexes, perhaps restoring those associated with cellular differentiation. These novel findings support a model in which SMARCB1 inactivation blocks the conversion of growth-promoting SWI/SNF complexes to differentiation-inducing ones, and they implicate SMARCB1 loss as a late event in tumorigenic progression. Importantly, the absence of growth inhibition after SMARCB1 restoration creates a unique opportunity to identify therapeutic vulnerabilities. *(Am J Pathol 2023, 193: 456–473; https://doi.org/10.1016/j.ajpath.2022.12.012)*

Chordomas are a rare and aggressive malignancy of the axial skeleton, originating from notochordal remnants in the axial skeleton. In the general population, the incidence of chordomas is <1 per 1 million, with approximately 95% of cases appearing in the older adult population.[1,2] Chordomas are classified according to histopathology into three subtypes: well-differentiated, poorly differentiated (PD), and de-differentiated.[3] Both well-differentiated and PD chordomas express brachyury, whereas de-differentiated tumors are characterized by loss of brachyury in the nonconventional components and are generally diagnosed after prior treatment. Regardless of subtype, the principal treatment of chordoma is surgical resection (often limited by critical neurovascular structures), augmented by adjuvant radiotherapy.[4] Only about 50% of chordomas respond well to cytotoxic therapy, radiation, and/or surgery. The identification of therapeutic targets has proven challenging due to the infrequent occurrence of clinically actionable somatic

Supported by NCI T32 CA 217824 (T.A.W.), NCI R01CA195670 (B.E.W.), T32ES007126 (B.V.), Terry Fox New Frontiers Program Project Grant #1082 (M.H.), and TFRI Forme Fruste grant (S.Y.).

Disclosures: S.Y. is a member of the advisory boards of Amgen, AstraZeneca, Bayer, Incyte, Novartis, Roche.

https://doi.org/10.1016/j.ajpath.2022.12.012

mutations, although mutations in *PIK3CA*, *EGFR*, and *PDGFR* may provide options for treatment in a subset of patients.[4–6] The combination of these factors contributes to an approximately 50% survival rate, highlighting an urgent need for identifying new treatments and improving patient outcomes.[7,8]

Although only 5% of chordomas occur in the pediatric and young adult population, approximately 15% of them are classified as PD chordomas.[1,2] Importantly, PD chordomas coincide with worse prognosis and a more aggressive clinical course,[9] with a propensity for metastasis and recurrence.[10] Studies have shown that PD chordomas possess inactivating mutations of *SMARCB1*, a key member of the Switch/Sucrose Non-Fermentable (SWI/SNF) chromatin remodeling complex.[5,11] Mutations in members of the SWI/SNF complex appear in approximately 20% of all cancers.[12] Defined by subunit composition, at least three distinct SWI/SNF complexes [BRG1/BRM-associated factor (BAF), polybromo-associated BAF (PBAF), and GLTSCR1/like-containing BAF (GBAF) complexes] exist in human cells, each imparting a specific effect on cell growth and differentiation.[13] Many SWI/SNF subunits are tumor suppressors for which loss of function drives oncogenic phenotypes in diverse cancers.[14] Evidence for inactivation of SMARCB1, a member of the BAF, PBAF complexes, as a driver of cancer was first documented in rhabdoid tumors (RTs), clinically aggressive tumors that arise in the kidney and the central nervous system.[15,16] SMARCB1 inactivation also drives the development of two other aggressive embryonal tumors of children and young adults: epithelioid sarcomas[17] and renal medullary carcinomas.[18] Recent genome-wide profiling studies have also identified SMARCB1 loss in other more "conventional" cancers exhibiting classical histology such as high-grade ovarian serous carcinoma, melanoma, and pancreatic ductal adenocarcinoma.[19–21] Yet, how the mechanisms by which loss of SMARCB1 fuels development of these tumors and PD chordomas remains unresolved.

The potential role of other driver mutations in the etiology of *SMARCB1*-deficient tumors remains unclear. These tumors are genetically simple and uniform, bearing no other recurrent driver mutations, with primarily diploid genomes.[22–24] RTs display loss of expression of the *CDKN2A* ($p16^{INK4A}$) tumor suppressor due to epigenetic silencing by the polycomb complex 2 (*PRC2*).[25] The induction of SMARCB1 in RTs leads to re-expression of $p16^{INK4A}$ through eviction of PRC2 leading to cell cycle arrest.[25,26] In contrast, all subtypes of chordomas exhibit inactivation or deletion of the *CDKN2A* gene.[5,27] The different mechanisms for silencing $p16^{INK4A}$ expression suggest that the pathways for tumorigenesis used among SMARCB1-deficient cancers may vary. To test this notion, the effects of SMARCB1 re-expression on the growth and gene expression of SMARCB1-deficient PD chordoma and RT cell lines were analyzed. The results show dramatic differences in how PD chordoma and RT cell lines respond to SMARCB1 re-expression. These findings support a model in which SMARCB1 inactivation blocks the conversion of growth-promoting SWI/SNF complexes to differentiation-inducing ones. In addition, the cell lines developed in the current study will contribute to the identification of therapeutic vulnerabilities for *SMARCB1* mutations across SWI/SNF cancers in humans.

Materials and Methods

Mammalian Cell Lines and Culture Conditions

The cell lines and their origins are listed in Table 1. The CH22, UM-Chor5, G401,[28,29] TTC642, D98OR,[30] BIN67,[31] COV434,[32] A427, and MCF7 cell lines were cultured in RPMI 1640 (#11875-093; Gibco, Grand Island, NY) and supplemented with 10% fetal bovine serum (FBS; Sigma-Aldrich, St. Louis, MO). The UM-Chor1 cells were cultured in Iscove's Modified Dulbecco's Medium (#12440-053; Gibco):RPMI 1640 (4:1) and supplemented with 10% FBS (Sigma-Aldrich). The MUG-Chor1 and U-CH17M cell lines were cultured in Iscove's Modified Dulbecco's Medium:RPMI 1640 (4:1), supplemented with 10% FBS (Sigma-Aldrich) and 1% GlutaMAX-I (100X) (#35050-061; Gibco). The pIND20-fSNF5-HA cell lines were cultured in RPMI 1640, supplemented with 10% TET-FREE FBS (#100-800; GeminiBio, Sacramento, CA) and 400 μg/mL G418/Geneticin 50 mg/mL (#10131-035; Gibco). The pLX401-INK4a cells were cultured in RPMI 1640, supplemented with 10% TET-FREE FBS (#100-800; GeminiBio) and 1 mg/mL puromycin (#50190304; MilliporeSigma, Laramie, WY). All cells were maintained in a humidified incubator at 37°C with 5% carbon dioxide. All were used within 10 passages of their initial arrival to minimize chances of cross-contamination and tested for mycoplasma contamination by DAPI staining and PCR for the detection of mycoplasma ribosomal DNA.

Inducible Cell Line Generation

pINDUCER20

Each cell line was infected with lentivirus containing pINDUCER20-Flag-SNF5-HA (pIND20-fSNF5-HA) as previously described.[33] After overnight incubation, cells were selected in RPMI 1640 medium supplemented with 10% TET-FREE FBS (#100-106; GeminiBio) + 400 μg/mL G418 (#10131035; Gibco) to create SMARCB1-inducible cell lines. Single-cell clones of each cell line were generated by limiting dilution and were screened for SMARCB1 expression after doxycycline (DOX) (1 μg/μL) induction for 24, 48, 72, 120, and 168 hours by Western blot analysis. Clones showing a robust induction of *SMARCB1* were pooled to create a mass pool of cells.

pLX401-INK4a

pLX401-INK4A was a gift from William Hahn (plasmid #121919; Addgene, Watertown, MA).[34] Cells were selected in RPMI 1640 media containing 10% TET-FREE FBS (#100-800; GeminiBio) + 1 mg/mL puromycin to create mass populations. For all pIND20 inductions, UM-Chor5, CH22, G401, and TTC642 pLX401-INK4a cells were induced with DOX 1 μg/μL for 72 hours before transfections. After selection, the mass population was single-cell cloned; using Western blot analysis, it was screened for $p16^{INK4A}$ expression following induction of DOX (1 μg/μL) for 24, 48, 72, 120, and 168 hours. Clones that could induce $p16^{INK4A}$ were pooled to create a mass pool of cells.

Protein Extraction

Cells (5 to 10 × 10^6), grown in a 60 mm dish, were washed twice with 10 mL of Dulbecco's Phosphate Buffered Saline (#14190-144; Gibco). The dish was then held at a 90-degree angle for 30 seconds for removal of residual Dulbecco's Phosphate Buffered Saline. Approximately 150 to 200 μL of 1X denaturing sample (250 mmol/L Tris 7.0, 8% SDS, 40% glycerol, 200 mmol/L dithiothreitol, 0.04% phenol red), based on the estimated number of cells, was added to the middle of the dish. Cells were removed with a cell lifter (#3008; Corning, Corning, NY) and collected in a 1.5 mL microcentrifuge tube. The extract was placed into a heat block for 7 minutes at 100°C. After allowing the sample to reach room temperature, DNA was sheared by sonication (Branson Ultrasonics Sonifier SFX150 Cell Disruptor; Thermo Fisher Scientific, Waltham, MA) on a low 100% duty cycle for 30 seconds, and processed samples were stored at −80°C until use.

Western Blot Analysis

Western blot analysis was performed as previously described.[33] Briefly, 3 to 4 μL of protein was separated on a Invitrogen NuPAGE 4 to 12% Bis-Tris Gel (#NP0322BOX; Thermo Fisher Scientific) in NuPAGE MOPS SDS Running Buffer (#NP0001; Thermo Fisher Scientific) at 130 V for 90 minutes. Proteins were transferred to a nitrocellulose membrane (#88018; Thermo Fisher Scientific) using 2X Bis-Tris Transfer Buffer (# BP-193; Boston BioProducts, Milford, PA) with 15% ethanol at 24 V for 1 hour. The efficiency of transfer was confirmed with Ponceau S staining. After blocking in 5% nonfat dry milk in 1X phosphate-buffered saline (PBS) for 1 hour, the membrane was washed using 1X PBS with Tween 20 (3 × 10 minutes), cut, and each section incubated overnight at 4°C in the primary antibodies listed in Table 2. After primary incubation, membranes were washed in 1X PBS with Tween 20 (3 × 10 minutes) and incubated in Li-COR Secondary Antibodies (IRDye 800CW; Goat anti-Rabbit, catalog #926-32211; Donkey anti-Mouse, catalog #926-32212; or 680RD Goat anti-rabbit, catalog #926-68071; Donkey anti-mouse: catalog #926-68072; Li-COR Biosciences, Lincoln, NE) diluted in 5% nonfat dry milk 1X PBS (1:10,000) for 1 hour at room temperature. Blots were washed with 1X PBS with Tween 20 (3 × 10 minutes) and imaged on an Odyssey machine (Li-COR Biosciences) at high quality at a resolution of 169 μm.

Immunoprecipitation

Small-scale nuclear extracts were prepared by using NE-PER Nuclear and Cytoplasmic Extraction (Thermo Fisher Scientific) following the manufacturer's specifications. Then, 150 μg of protein was incubated with antibodies to ARID1A, BAF180, SMARCA4, GLTSCR1, or IgG, rotating overnight at 4°C with 30 μL of a 50% slurry of protein A/G Sepharose beads (GE Healthcare Bio-Sciences, Piscataway, NJ). After washing three times with immunoprecipitation wash buffer (1X PBS, 10% glycerol, and 1% Triton), the beads were suspended in 1X NuPAGE LDS Loading Buffer (Thermo Fisher Scientific) supplemented with 1.0 mol/L dithiothreitol and placed in a heat block at 95°C for 5 minutes. The supernatants were run on a 4% to 12% Bis-Tris polyacrylamide gel, transferred to a nitrocellulose membrane, and probed with anti-BRG1, anti-PBRM1, anti-ARID1A, anti-GTLSCR1, anti-BRD9, and anti-SMARCB1 as described in *Western Blot Analysis*.

Epigenetic Inhibitor Assays

For assessing SMARCA2 expression after treatment with epigenetic inhibitors, cells were seeded into 10 cm dishes at 2 × 10^5 per dish and incubated overnight. Cells were then treated with 10 nmol/L quisinostat (#JNJ-26481585; Pfizer, New York, NY), 10 μmol/L UNC1999 (University of North Carolina, Chapel Hill, NC) or GSK126 (#S7061; Selleck Chemicals, Houston, TX), or 10 μmol/L dimethyl sulfoxide (#D128-500; Fisher Chemical, Fair Lawn, NJ) for 5 days. Untreated cells served as controls. Each drug was added/replaced along with media replacement on days 1 and 3. The cells were harvested by sample buffer protein extraction on the fifth day. Western blot analysis was used to quantify the re-expression of SMARCA2 protein. The experiment was completed with three biological replicates.

For determining the effects of epigenetic inhibitors on cellular proliferation, cells were seeded into 24-well dishes at 2.5 × 10^4 per well. Plates were imaged at 4X the following day (day 1). Increasing concentrations of quisinostat or GSK-126 were applied to the 24-well plates in RPMI 1640 media + 10% FBS, with untreated and dimethyl sulfoxide—treated wells serving as controls. Four technical replicates per dose and three overall biological replicates for each cell line and treatment were used. A media change was done on day 3. After viewing cells on day 7, cells were fixed with 0.75 mL per well of 10% methanol/10% acetic acid solution for 10 minutes. Cells were stained with 0.25 mL per well of 0.5% crystal violet in methanol for 10 minutes and

Table 1 Cell Line Characteristics

Cell lines	Disease origin	Age, years	Source	*SMARCB1* expression	*SMARCA4* expression	*SMARCA2* expression
CH22	Sacral chordoma	56	Chordoma Foundation	No	Yes	No
UM-Chor5	Clival chordoma	<20	Chordoma Foundation	No	Yes	No
G401.6	Rhabdoid tumor	<1	28,29	No	Yes	No
TTC642	Rhabdoid tumor	Unknown	Dr. Tim Triche, Children's Hospital Los Angeles	No	Yes	No
D98OR (HeLa)	Cervical carcinoma	31	30	Yes	Yes	Yes
BIN67	Small carcinoma of the ovary, hypercalcemic type	Unknown	31	Yes	No	No
COV434	Small carcinoma of the ovary, hypercalcemic type	26	32	Yes	No	No
A427	Lung adenocarcinoma	52	ATCC	Yes	No	No
MCF7	Breast adenocarcinoma	69	ATCC	Yes	Yes	Yes
UM-Chor1	Clival chordoma	66	Chordoma Foundation	Yes	Yes	Yes
MUG-Chor1	Sacral chordoma	57	Chordoma Foundation	Yes	Yes	Yes
U-CH17M	Sacral chordoma	38	Chordoma Foundation	Yes	Yes	Yes

then washed with double-distilled water to remove excess crystal violet. Once plates had dried, 0.75 mL of methanol + 0.1% SDS was added to each well to resolubilize the stained cells using a rocker for 2 hours. After rocking, 15 μL of each sample was diluted 1:10 in 135 μL of resolubilization solution (methanol + 0.1% SDS) in a 96-well plate. Resolubilization solution was added to four wells as a control. Absorbance was measured at 595 nm. Background signal from the resolubilization solution was subtracted from sample absorbance readings. Optical density was calculated by dividing the average absorbance for each dose of quisinostat or GSK-126 by the average absorbance of the untreated control wells. Paired *t*-tests were performed according to dose and cell line for statistical analysis.

Cell Growth Assays

Cells were seeded into 24-well plates at 1×10^3 per dish and placed in the IncuCyte S3 Live-Cell Analysis System (Essen BioScience, Ann Arbor, MI) for 7 days. Cells were induced for SMARCB1 expression by treatment with DOX 1 μg/μL (#PHR1145-1G; MilliporeSigma, Laramie, WY). Continuous live content was captured by 10X phase images of the wells every 4 hours. Treatments were added and

Table 2 Antibodies

Antibody	Source	Dilution	Identifier
Rabbit Anti-ARID1A (BAF250A) (D2A8U) (IP/WB)	Cell Signaling Technology	1:1000	Catalog #12354
Rabbit Anti-BAF57 (WB)	Bethyl Laboratories	1:1000	Catalog #300-810A
Mouse Anti-SMARCD1 (BAF60A) (23) (WB)	Bethyl Laboratories	1:1000	Catalog #A301-595A
Mouse Anti-SMARCC1 (BAF155) (DXD7) (WB)	Sigma (Darmstadt, Germany)	1:1000	Catalog #85186
Rabbit Anti-SMARCC2 (BAF170)	Bethyl Laboratories	1:1000	Catalog #A301-038A
Mouse Anti-PBRM1 (BAF180) (IP/WB)	Cell Signaling Technology	1:1000	Catalog #818325
Rabbit Anti-BRD7 (WB/IP)	Bethyl Laboratories	1:2000	Catalog #A302-304A
Rabbit Anti-BRD9 (WB)	Abcam (Cambridge, UK)	1:1000	Catalog #ab137245
Rabbit Anti-CDKN2A ($p16^{INK4A}$) (WB)	Abcam	1:2000	Catalog #ab108349
Mouse Anti-CD44 (WB)	A gift from Dr. Larry Sherman, University of Oregon Health Sciences Center	1:250	
Rabbit Anti-GLTSCR1 (IP/WB)	Sigma	1:1000	Catalog #HPA056211
Rabbit Anti-IgG (IP)	Cell Signaling Technology	2 μg	Catalog #27295
Rabbit Anti-Ku 70/80 (WB)	A gift from Dale Ramsden, University of North Carolina	1:250	
Rabbit Anti-SMARCA2 (BRM) (WB)	Cell Signaling Technology	1:1000	Catalog #119665
Rabbit Anti-SMARCA4 (BRG1) (EPNCIR111A) (IP/WB)	Abcam	1:10,000	Catalog #ab110641
Mouse Anti-SMARCB1 (SNF5) (WB)	BD Biosciences, Franklin Lakes, NJ	1:1000	Catalog #612110
Rabbit Anti-SMARCB1 (IP)	Bethyl Laboratories	2 μg	Catalog #A301-087A
Rabbit Anti-HA tag (WB)	Cell Signaling Technology	1:1000	Catalog #3724T

IP, immunoprecipitation; WB, Western blot analysis.

media refreshed on days 1, 3, and 5. Growth assays were completed with three biological replicates. The statistical quantification was completed by the basic analyzer function. The average of the three biological replicates was used to generate the growth curve in GraphPad Prism 8 (GraphPad Software, San Diego, CA).

Quantitative Real-Time PCR

Inducible cell lines were treated with DOX 1 μg/μL for 72 hours, harvested by treatment with 0.25%/0.01% trypsin/EDTA, washed with PBS, and frozen rapidly by exposure to liquid nitrogen. RNA was extracted from frozen cell pellets in biological triplicate using the Quick-RNA Miniprep Kit (catalog #R1054; Zymo Research, Irvine, CA). Total RNA was converted to cDNA using the iScript Reverse Transcription Kit (Bio-Rad, Hercules, CA). cDNA levels were quantified by using PowerUp SYBR Green Master Mix (#10002984; Applied Biosystems, Carlsbad, CA). Quantitative real-time PCR was performed on QuantStudio 6 Flex (Applied Biosystems). The results were analyzed by using a $2^{(-\Delta\Delta CT)}$ comparative method. Each sample was tested in triplicate. All primers are listed in Table 3.

RNA-Sequencing Samples and Analysis

Samples

For all RNA-sequencing studies, 2×10^6 CH22 and UM-Chor5 pIND20-fSNF5-HA cells were plated into 10 cm dishes and induced with DOX 1 μg/μL for 72 hours. RNA was extracted from frozen cell pellets in biological triplicate using the Quick-RNA Miniprep Kit (catalog #R1054; Zymo Research). Library preparations and RNA-sequencing were performed by Novogene Inc. (Beijing, China). Total RNA was prepared by Novogene Inc. using the TruSeq mRNA v2 kit (Illumina, San Diego, CA) with an input of 500 ng of RNA for each sample to produce unstranded RNA libraries following the manufacturer's protocol. Final RNA libraries were quantified by using the Qubit High Sense Reagent kit (Thermo Fisher Scientific) and TapeStation HSD1000 tapes (Agilent Technologies, Santa Clara, CA). Libraries were equimolar pooled and paired-end sequenced across three lanes of a HiSeq 4000 system (paired-end ×78 bp; Illumina).

For TTC642 pIND20-fSNF5-HA, cells were treated, with or without DOX 1 μg/μL for 72 hours. Cells were then harvested, RNA isolated, and sequenced as previously described.[35]

RNA-sequencing for the CH22 and UM-Chor5 pIND20-fSNF5-HA cells, and TTC642 pIND20-fSNF5-HA cells, with or without DOX, were deposited in the NIH Gene Expression Omnibus (*https://www.ncbi.nlm.nih.gov/geo*; accession number GSE217999). For G401 pIND20-fSNF5-HA, RNA-sequencing data were accessed from the NIH Gene Expression Omnibus (*https://www.ncbi.nlm.nih.gov/geo*; accession numbers GSE90633 and GSE71506).

Table 3 Quantitative Real-Time PCR Primers

Gene ID	Primer sequence
SMARCA4	FWD: 5′-AGGCGCCGGGAAGTCGATGG-3′
	REV: 5′-CCATCGACTTCCCGGCGCCT-3′
SMARCA2	FWD-5′-TCCGAGGCAAAATCAGTCAAG-3′
	REV: 5′-TTCCTCGATTTGGCCTTTTCT-3′
SMARCB1	FWD: 5′-ATCACGGATACACGACTCTAGC-3′
	REV: 5′-CACGGCATCTAAGTGGTGG-3′
GAPDH	FWD: 5′-ATGGGGAAGGTGAAGGT-3′
	REV: 5′-AAGCTTCCCGTTCTCAG-3′
CDKN2A^{p16INK4A}	FWD: 5′-GGGTTTTCGTGGTTCACATCC-3′
	REV: 5′-CTAGACGCTGGCTCCTCAGTA-3′

FWD, forward; REV, reverse.

Analysis

Reads were trimmed by using cutadapt (version 1.12)[36] using options -a GATCGGAAGAGC -A GATCGGAAGAGC and –minimum-length 36 to remove any sequencing adapters. After trimming, reads were filtered for quality using the fastq_quality_filter in FASTX-Toolkit (version 0.0.12; (*http://hannonlab.cshl.edu/fastx_toolkit*), with options -Q 33, -p 90, and -q 20 -. Cell lines JHC7, MUG-Chor1, U-CH1, U-CH2, and UM-Chor1 were run with option -Q 64 instead. Reads were aligned to the hg19 genome using STAR (version 2.5.4b)[37] with options –quantMode TranscriptomeSAM, –outFilterMismatchNmax 2, –alignIntronMax 1000000, –alignIntronMin 20, –chimSegmentMin 15, –chimJunctionOverhangMin 15, –outSAMtype BAM Unsorted, –outFilterType BySJout, and –outFilterMultimapNmax 1.

To calculate the RNA abundance values in transcripts per million, Salmon (version 0.8.1)[38] tool quant was used. Samtools (version 1.3.1),[39] bedtools (version 2.26),[40] Python (version 3.7.9),[41] and R (version 3.3.1)[42] were used to interconvert files for downstream analyses. DESeq2 (version 1.14.1)[43] was used to determine which genes had significantly differential RNA abundance.

Principal component analysis (PCA) plots were generated by using the plotPCA function within DESeq2 using all RNA abundance values (transcripts per million). g:Profiler GOSt was used to identify Reactome pathways and *P* values associated with differentially expressed genes.[44,45] Heatmaps of gene transcripts per million were made using Morpheus (*https://software.broadinstitute.org/morpheus*, last accessed January 3, 2021). Boxplots were made in Python with seaborn boxplot and stripplot commands using the $\log_2$ fold changes between the mean transcripts per million across replicates between *SMARCB1*-positive and *SMARCB1*-negative samples.[41,46] UpSet plot was generated in R with the UpSetR package.[47]

Senescence Assay

Cells (1×10^5 cells per well) were plated in a six-well dish and treated with or without DOX for up to 7 days.

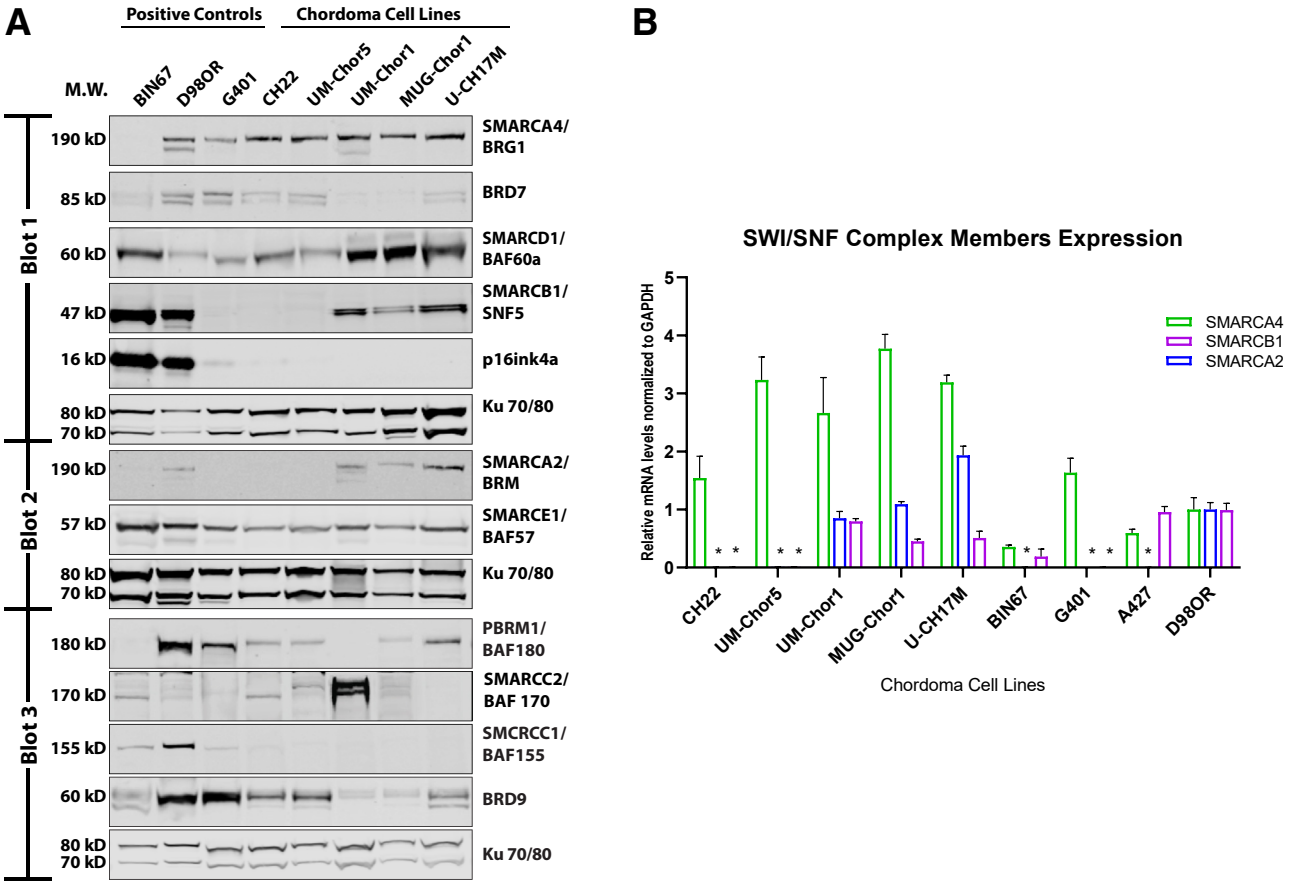

Figure 1 Characterization of Switch/Sucrose Non-Fermentable (SWI/SNF) complex members in poorly differentiated chordomas. **A:** Protein expression levels in chordomas, rhabdoid tumor, HeLa, and small cell carcinoma of the ovary. Antibodies against SWI/SNF complex members were used. Ku 70/80 was used as the loading control. **B:** Relative mRNA levels in the indicated cell lines. mRNA levels were measured for *SMARCA4* (**green**), *SMARCA2* (**blue**), and *SMARCB1* (**violet**) genes by using real-time quantitative PCR and normalized to D98OR GAPDH expression. *Gene expression detection was below the threshold. M.W., molecular weight.

Senescence was assessed with the Senescence β-Galactosidase Staining Kit without modifications (Cell Signaling Technology, Danvers, MA). The percentage of β-galactosidase–positive cells was quantified by averaging the cell count taken from 10 random fields.

Immunohistochemistry

Immunohistochemistry (IHC) was performed by using anti-brachyury (Clone H-210, primary dilution 1:400, sc-20109; Santa Cruz Biotechnology, Santa Cruz, CA), anti-SMARCB1 (Clone 25/BAF47, primary dilution 1:100, 612110; BD Transduction), anti-SMARCA2/BRM (primary dilution 1:200, HPA029981; Sigma), anti-SMARCA4/BRG1 (EPNCIR111A, primary dilution 1:200, ab110641; Abcam, Cambridge, UK) on a BOND platform (Leica Biosystems, Wetzlar, Germany). Tissue microarray of 0.6 mm^2 duplicate cores were constructed from formalin-fixed, paraffin-embedded tissue chordoma specimens at Vancouver General Hospital. The project was approved by the Vancouver General Hospital Research Ethics Board. SMARCB1, SMARCA2, and SMARCA4 IHC was conducted as previously described.[48] Brachyury IHC was performed by using rabbit polyclonal antibody at 1:50 dilution (sc-20109; Santa Cruz Biotechnology), and PBRM1 IHC was performed by using rabbit polyclonal antibody at 1:1000 dilution (A301-591A; Bethyl Laboratories, Montgomery, TX); both were run by using the Ventana Discovery Ultra platform (Roche Holding AG, Oro Valley, AZ). All photomicrographs were taken at ×100 magnification. Staining was evaluated by a pathologist (S.Y.).

Statistical Analysis

A one-sample *t*-test of all samples was performed to determine whether the sample mean is statistically different from zero, which means no change. A P value <0.05 was considered significant. GraphPad Prism 8 software (GraphPad Software, San Diego, CA) was used to present the data. To evaluate the effect of the epigenetic inhibitors on each cell line (CH22, UMCHOR5, and COV434), paired *t*-tests were performed by comparing the optical density of

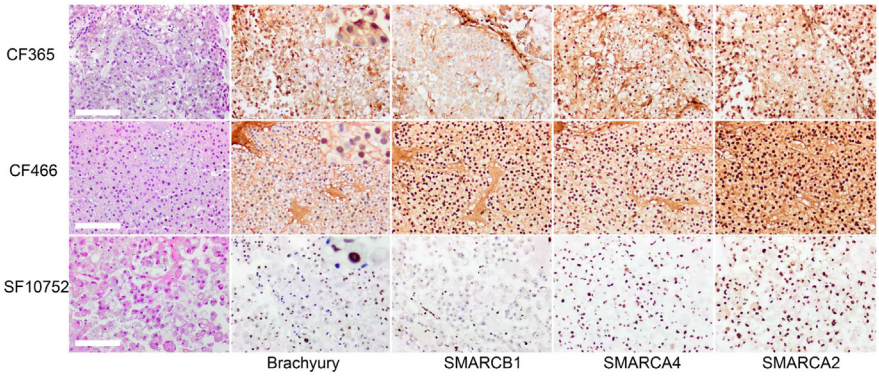

Figure 2 Immunohistochemistry analyses of poorly differentiated chordomas. Immunohistochemistry of patient-derived xenograft from clinical chordoma specimens confirmed positive nuclear expression of brachyury in all three samples. CF365 and SF10752 were derived from poorly differentiated chordoma, and both show loss of nuclear expression of SMARCB1. CF466 was derived from a well-differentiated chordoma and shows retention of SMARCB1 expression. All three cases, regardless of SMARCB1 expression status, show retention of SMARCA4 and SMARCA2 expression. Scale bars = 100 μm. Original magnification, ×100.

the untreated control replicates with the epigenetic inhibitor-exposed replicates at each dose (50, 20, 10, 5 nmol/L for quisinostat, and 20, 10, 5 μmol/L for GSK-126) for each cell line. To evaluate the effect of the epigenetic inhibitors across cell lines, paired *t*-tests were used to compare the optical density of the replicates by cell line for each dose of quisinostat or GSK-126 as well as the untreated controls.

Results

SWI/SNF Mutant–Cancers Differ in SWI/SNF Complex Member Expression

A key feature of the SWI/SNF complex is its highly combinatorial nature.[49] The absence of SMARCB1 in RT cell lines leads to instability of the BAF and PBAF complexes but not the GBAF complex.[33,50,51] Therefore, the expression and composition of SWI/SNF complex subunits were initially characterized in PD chordomas. The SWI/SNF component expression was first examined in both SMARCB1-negative and SMARCB1-positive chordoma cell lines (Figure 1A). The chordoma protein expression levels were compared versus two previously characterized SWI/SNF–mutant cancers, BIN67 [small cell carcinoma of the ovary, hypercalcemic type (SCCOHT)][48] and G401 (RT),[16] with known deletions or inactivation in the ATPase subunit *SMARCA4* (BRG1) and *SMARCB1*, respectively. D98OR, a HeLa cell derivative, served as a positive control for the expression of SWI/SNF complex components.[30,52]

All cell lines, except BIN67, expressed the SMARCA4 ATPase subunit (Figure 1A). SMARCA2 expression of the SMARCB1-negative CH22 and UM-Chor5 chordomas was not observed, similar to previous reports showing SMARCA2 loss in SMARCB1-negative RT (G401) and SMARCA4^{neg} (BIN67) cell lines.[48,53] However, the three SMARCB1-positive chordomas (UM-Chor1, MUG-Chor1, and U-CH17M) and D98OR expressed SMARCA2. As expected, SMARCB1 expression was not observed in the RT and the SMARCB1-negative chordoma cell lines (Figure 1A). Of import, SMARCC1 was not detected in any of the chordomas, in contrast to the SCCOHT and RT cell lines. SMARCC2 expression varied among the chordoma cell lines, with the highest levels found in UM-Chor1 and an undetectable amount in U-CH17M. All cell lines expressed BRD7, BRD9, SMARCD1, and SMARCE1, albeit at differing levels. Finally, all chordomas expressed lower levels of BAF180 (PBRM1) compared with D98OR except UM-Chor1, which possesses a truncating mutation in this gene.

Whether the absence of SMARCA2 protein in the CH22 and UM-Chor5 cell lines reflected changes in mRNA expression was explored next. Previous studies have shown that loss of SMARCA2 expression in SMARCB1- and SMARCA4-deficient cell lines results from epigenetic silencing of the gene.[48,53] Therefore, real-time quantitative PCR was used to measure RNA expression, normalized to positive control, the HeLa-derived D98OR cell line (Figure 1B). The SMARCA4/A2^{neg} cell line, A427 (lung adenocarcinoma), was also included as a second control for silencing of *SMARCA2* gene expression.[54] Consistent with the Western blot data, SMARCB1 mRNA expression was undetectable in the CH22, UM-Chor5, and RT cell lines. SMARCA4 and SMARCA2 mRNA expression levels were also consistent with observed protein expression levels in the cell lines. Because DNA sequencing revealed no mutations in the SMARCA2 gene in CH22 or UM-Chor5, these results implicate gene silencing as the likely mechanism for the loss of expression.

Lack of SMARCB1 expression in RTs, previously characterized by a breadth of histologic and immunohistochemical approaches, are nearly all caused by mutation, deletion, loss of, or reduced RNA expression of the *SMARCB1* gene found on chromosome 22q11.2.[55–57] Given that loss of SMARCB1 expression at the protein level is nearly universal in RTs, loss of SMARCB1 protein expression by IHC has become a highly sensitive tool for

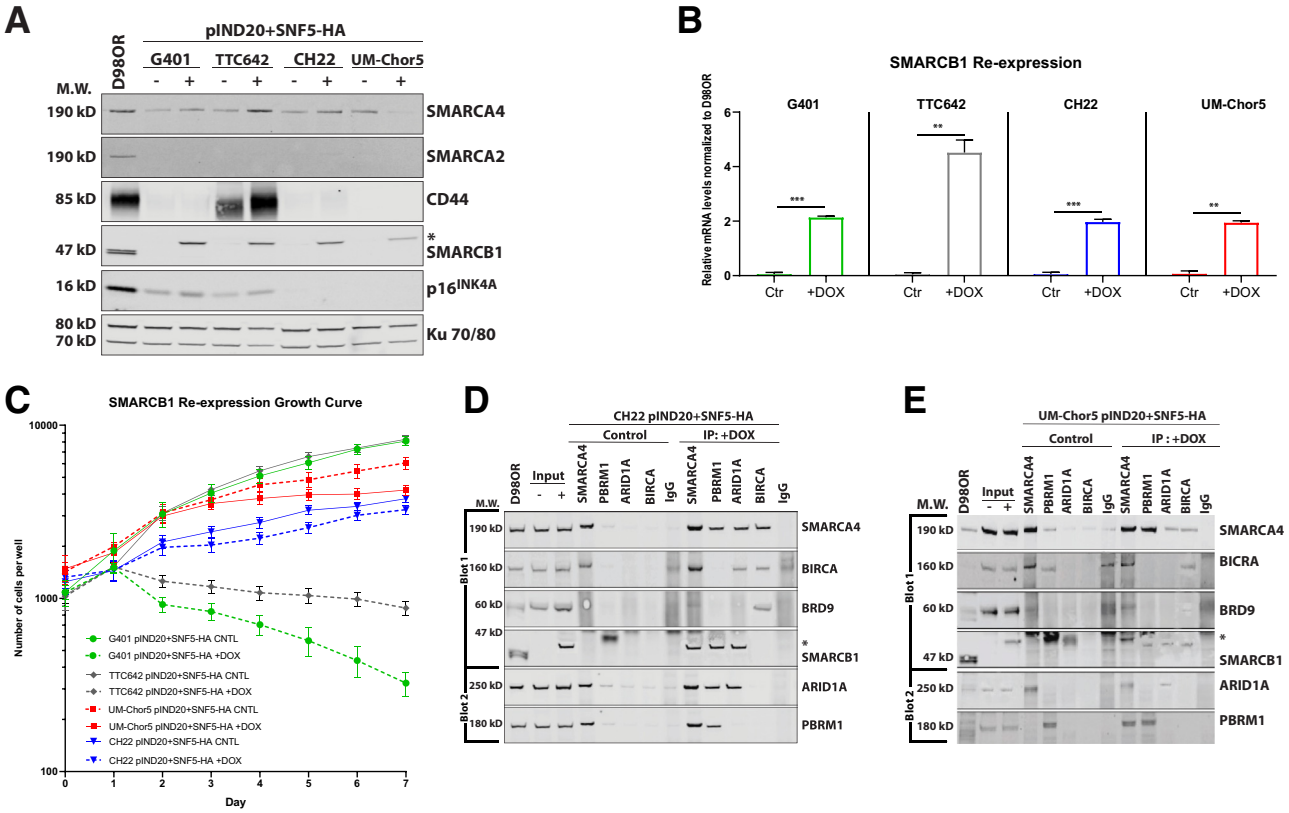

Figure 3 SMARCB1 re-expression in SMARCB1-negative chordomas. **A:** Western blot indicating the effects of SMARCB1 protein expression on the levels of both SWI/SNF ATPase subunits, $p16^{INK4A}$, and CD44 proteins in the PD chordoma (CH22 and UM-Chor5) and RT (G401 and TTC642) cell lines 72 hours after DOX induction. Ku 70/80 was used as the loading control. **B:** Relative mRNA levels for *SMARCB1* 72 hours after DOX induction using real-time quantitative PCR and normalized to D98OR GAPDH expression. The results confirm the induction of SMARCB1 protein in **panel A** came from transcription of the SMARCB1 transgene. **C:** Growth curves demonstrate that SMARCB1 re-expression inhibits proliferation of the RT (G401 and TTC642) but not the PD chordoma (CH22 and UM-Chor5) cell lines. Treatment of 1 μg/mL doxycycline (DOX) was added on days 1, 3, and 5. Media were replaced in untreated control wells on days 1, 3, and 5. The growth curve is the average of three biological replicates on a log scale. **D** and **E:** SMARCB1 protein expression leads to reconstitution of the three major subtypes of SWI/SNF complexes. Total nuclear protein from indicated cell lines immunoprecipitated with either rabbit IgG, anti-BRG1, anti-PBRM1, anti-ARID1A, or anti-GLTSCR1 in the presence or absence of SMARCB1 protein expression. The expression of SWI/SNF subunits SMARCA4, BIRCA, BRD9, SMARCB1 was detected by Western blot analysis (Blot 1). The Western blots were then stripped and re-probed for the ARID1A and PBRM1 subunits (Blot 2). *Larger molecular weight (M.W.) form of the SMARCB1 protein due to the addition of the HA and flag tags. *t*-test was performed: $^{**}P < 0.01$, $^{***}P < 0.001$. −, untreated control; +, treated with DOX (1 μg/mL); Ctr, no DOX.

diagnosis of this tumor.[57] Therefore SMARCB1 status was examined in chordoma tumor samples taken from both pediatric and adult patients. As expected, seven well-differentiated chordomas showed positive labeling for BRACHYURY and four SWI/SNF complex subunits, including SMARCB1 (Supplemental Figure S1). A similar result using a well-differentiated chordoma provided by the Chordoma Foundation (Figure 2), CF466, was also observed. Surprisingly, both SMARCB1-negative PD chordomas, CF365 and SF10752, retained expression of SMARCA4 and SMARCA2 (Figure 2). A third SMARCB1-negative PD chordoma sample, CHOP 13425-159, also expressed SMARCA2 (Supplemental Figure S2). The expression of SMARCB1 in normal endothelial cells provides an internal positive control for the IHC. Because the SMARCA2-negative UM-Chor5 cell line did not express SMARCA2, the current results implicate the loss of SMARCA2 expression as an event during establishment of this cell line.

SMARCB1 Re-Expression Does Not Inhibit Chordoma Proliferation

Re-expression of SMARCB1 in RT cell lines inhibits their growth within 48 hours.[58,59] To determine the effects of SMARCB1 re-expression of the growth of SMARCB1-negative chordoma cell lines, the previously described DOX-inducible SMARCB1 vector (pIND20-fSNF5-HA) was introduced into the CH22 and UM-Chor5 cell lines (CH22 and UM-Chor5) (Figure 3).[33] Although most cell lines, such as D98OR, express two splice forms of the SMARCB1 (Figure 3A), herein, the larger splice form was expressed, which was used in most studies. A single protein was observed after re-expression of SMARCB1 with a larger molecular weight due to the addition of the HA and flag tags. The levels of SMARCB1 expression were characterized by using Western blot analysis and real-time quantitative PCR after induction from 24 hours up to 7 days to show that the PD chordoma and RT cells expressed

SMARCB1 mRNA levels similar to cells with a wild-type *SMARCB1* gene (D98OR).

SMARCB1 protein expression was compared between the PD chordoma (CH22 and UM-Chor5) and RT (G401 and TTC642) cell lines 72 hours after DOX induction (Figure 3A). SMARCA4 protein levels did not change significantly after SMARCB1 re-expression. Induction of SMARCA2 was not observed in any of the cell lines. Next, SMARCB1 re-expression was confirmed at the mRNA level by using real-time quantitative PCR (Figure 3B). The re-expression of SMARCB1 was statistically significant in all the cell lines. As previously reported, induction of $p16^{INK4A}$ was observed in the RT cell lines.[58] As expected, no expression was observed in the $p16^{INK4A}$-deficient PD chordoma cells. Finally, the expression of a known downstream target of the SWI/SNF complex, CD44, was examined.[60] CD44 is a well-characterized cell surface receptor with several isoforms expressed in epithelial cells.[61,62] Although SMARCB1 re-expression appeared to increase CD44 in the TTC642 RT cell line, re-expression was not found in the CD44-negative G401 RT and PD chordoma cell lines (Figure 3A). Finally, assembly of the SWI/SNF complex after SMARCB1 re-expression in the CH22 and UM-Chor5 cell lines was confirmed by immunoprecipitation (Figure 3, C and D).

The growth of the PD chordoma pIND20-fSNF5-HA cell lines versus two previously engineered RT cell lines, G401- and TTC642-pIND20-fSNF5-HA, after SMARCB1 re-expression was compared next. Growth was measured over 7 days using live cell content capture quantification by IncuCyte (Figure 3E).[63] The results confirmed previous reports of decreased rates of proliferation in RT cell lines within 48 hours of SMARCB1 re-expression.[33] Interestingly, SMARCB1 induction in the chordoma cell lines had little effect on cell proliferation, as evidenced by their continued growth. The absence of growth arrest after SMARCB1 re-expression in PD emphasizes the different roles of SMARCB1 loss in the tumor versus RTs and provides a new model system to identify the biological mechanisms by which loss of SWI/SNF function fuels tumorigenesis.

SMARCB1 Re-Expression SWI/SNF Complex Formation in Chordomas

Complete BAF and PBAF subtypes fail to form in SMARCB1-deficient RT cell lines due to degradation of multiple components.[33,50,51] Therefore, immunoprecipitation of four SWI/SNF components, BRG1, PBRM1, ARID1A, and GLTSCR1, was performed in the presence or absence of SMARCB1 followed by Western blot analysis to determine the composition of the complexes (Figure 3, D and E). Nuclear extracts were isolated from the two chordoma pINDUCER cell lines, CH22 and UM-Chor5, and characterized by immunoprecipitation/Western blot analysis as previously described.[33]

Because SMARCA4 is present in all three complexes (BAF, PBAF, and GBAF), it immunoprecipitated regardless of SMARCB1 expression, as expected (Figure 3, D and E). In contrast, ARID1A (present in BAF complexes) and PBRM1 (present in PBAF complexes) only co-immunoprecipitated with SMARCA4 after SMARCB1 re-expression in the CH22 cell line (Figure 3D). Similar results were seen for the UM-Chor5 cell line except that ARID1A still co-immunoprecipitated with SMARCA4 in the absence of SMARCB1 (Figure 3E). These findings confirmed that, as with RTs, SMARCB1 loss impaired the assembly of BAF and PBAF complexes in PD chordoma. Unexpectedly, more GBAF complex was immunoprecipitated, identified by the presence of GLTSCR1 and BRD9, after SMARCB1 re-expression. However, GLTSCR1 did not pull down SMARCB1. The PBRM1 antibody immunoprecipitated ARID1A after SMARCB1 re-expression in the CH22, an unexpected result because the subunits appear in different complexes in a mutually exclusive manner (Figure 3D). Further studies are required to determine whether this finding represents a phenomenon specific to the CH22 cell line. However, the immunoprecipitation results indicate that SMARCB1 loss causes a similar loss of intact BAF and PBAF complexes in both chordomas and RT cell lines.

Chordomas Continue to Grow after $p16^{INK4A}$ Expression

Re-expression of SMARCB1 in RT cell lines leads to cell cycle arrest by evicting the polycomb complex 2 from the $p16^{INK4A}$ promoter and activating its expression.[25] However, growth arrest was not observed after SMARCB1 re-expression in the chordoma cell lines (Figure 3C). In contrast to RTs, a recent report showed that most primary chordomas do not express $p16^{INK4A}$/CDKN2A due to gene mutation/deletion rather than epigenetic silencing.[64] Therefore, the effects of $p16^{INK4A}$ re-expression were determined on our panel of SMARCB1-negative PD and RT cell lines. To accomplish this goal, CH22 and UM-Chor5 PD and G401 and TTC642 RT cell lines were generated with an inducible $p16^{INK4A}$ expression using the (pLX401-INK4a) expression vector.

The absence of $p16^{INK4A}$ expression in the PD chordomas was confirmed by Western blot analysis (Figure 1A). Next, re-expression of $p16^{INK4A}$ protein and mRNA expression were confirmed after 72 hours of induction in the CH22, UM-Chor5, G401, and TTC642 cell lines (Figure 4, A and B). Protein levels for SMARCA4 were not affected by $p16^{INK4A}$ re-expression. As expected, the expression of $p16^{INK4A}$ did not induce *SMARCB1* expression in the indicated cell lines.

The effect of $p16^{INK4A}$ re-expression on cell cycle regulatory genes (Figure 4C) and cellular growth (Figure 4D) was assessed next. Induction of $p16^{INK4A}$ in RTs caused decreased protein expression of cyclin-A and phosphorylated Rb (Figure 3D). This was in contrast with the PD

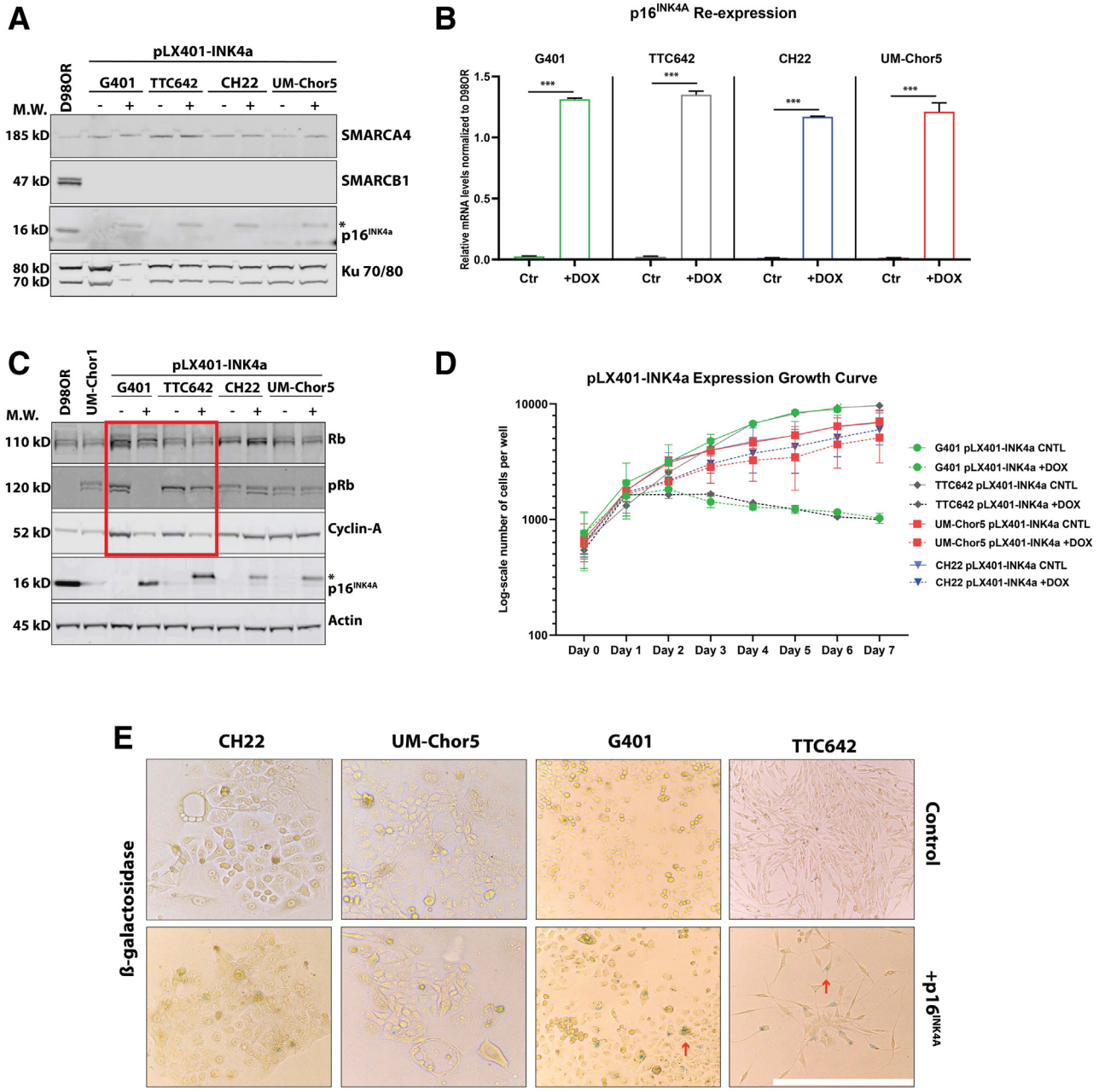

Figure 4 p16^{INK4A} re-expression in chordomas and rhabdoid tumors (RTs). **A:** Western blot indicating the p16^{INK4A} expression in the PD chordomas. Cells were harvested at 72 hours after induction of p16^{INK4A}. Ku 70/80 was used as the loading control. **B:** Real-time quantitative PCR results indicating re-expression of p16^{INK4A} mRNA expression after 72 hours of induction in the CH22, UM-Chor5, G401, and TTC642 cell lines. Raw data normalized to GAPDH expression. **C:** Western blot indicating the effect of p16^{INK4A} re-expression on cell cycle regulatory genes 72 hours after induction of p16^{INK4A}. Actin was used as the loading control. The **red box** highlights the reduced expression of phosphorylated Rb (pRb) and cyclin-A in the RT cell lines after p16^{INK4A} re-expression. **D:** Growth curve of the indicated cell lines indicating the effect of p16^{INK4A} re-expression. Cells were placed in IncuCyte for 7 days. Treatment of 1 μg/mL doxycycline (DOX) was added on days 1, 3, and 5. Media were replaced in untreated control wells on days 1, 3, and 5. The growth curve is the average of three biological replicates on a log scale. **E:** RT cell lines show evidence of senescence by β-galactosidase expression after the re-expression of p16^{INK4A}. Images are representative of 3 biological replicates. **Arrows** indicate β-galactosidase—positive cells. *Larger molecular weight (M.W.) form of the p16^{INK4A} protein due to the addition of a 6XHis tag. *t*-test was performed: ***$P < 0.001$. Scale bar = 270 μm. −, untreated control; +, treated with DOX (1 μg/mL); Ctr, no DOX.

chordomas, whereby the re-expression of p16^{INK4A} caused little to no change in protein levels of phosphorylated Rb or cyclin-A, suggesting that PD chordomas remain in a state of active cell cycle progression. To determine the effect of p16^{INK4A} re-expression on the growth, a 7-day live content capture growth assay was quantified by using the IncuCyte system (Figure 4D). Within 48 hours of p16^{INK4A} induction, there was a decrease in proliferation of both RTs along with

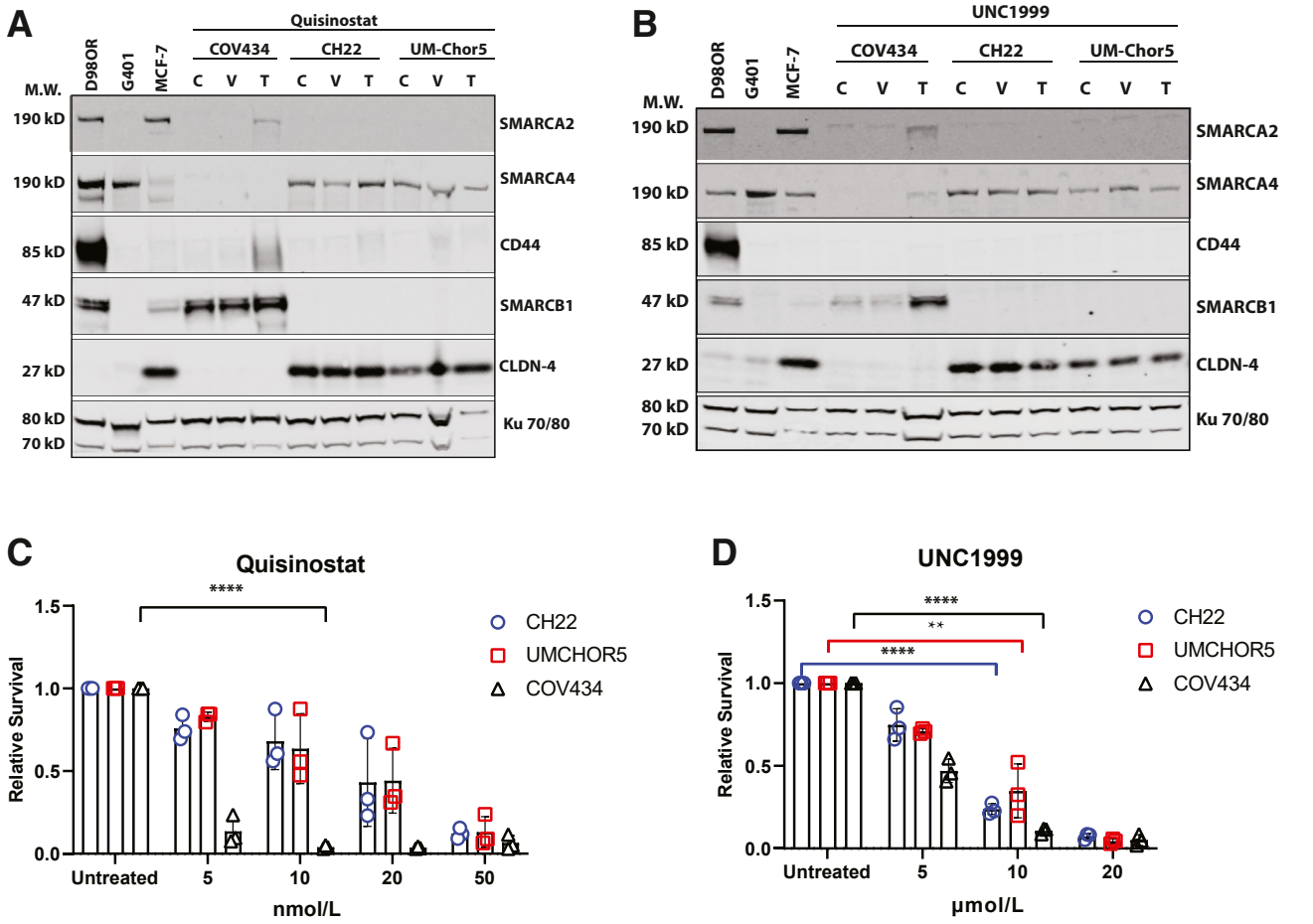

Figure 5 Re-expression of SMARCA2 with epigenetic inhibitors. **A** and **B:** Western blots indicating re-expression of SMARCA2 in SCCOHT and chondroma cell lines in the presence of HDAC or EZH1/2 inhibitors. Cells were treated with dimethyl sulfoxide (DMSO), 10 nmol/L histone deacetylase (quisinostat), or 10 μmol/L enhancer of zeste homolog 2 inhibitor (UNC1999) for 5 days. Ku 70/80 was used as the loading control. C indicates untreated cells; V indicates DMSO; and T indicates epigenetic inhibitor. **C** and **D:** Relative survival of CH22, UM-Chor5, and COV434 cells in the presence of the histone deacetylase inhibitor (quisinostat) (**C**) or enhancer of zeste homolog 2 inhibitor (UNC1999) (**D**). Cells were treated for 7 days with DMSO vehicle; 0, 10, 20, and 50 nmol/L quisinostat; or 0, 5, 10, 20 μmol/L UNC1999 equivalent to GSK-126. Paired *t*-tests were performed according to dose and cell line for statistical analysis: $^{**}P < 0.01$, $^{****}P < 0.0001$. There were no significant differences between the results for 0 and 50 nmol/L quisinostat for the CH22 and UM-Chor5 cell lines.

a change in cellular morphology, suggestive of senescence, as indicated in previous reports[58] (Figure 4E). This contrasts with the novel observation that PD chordomas are still proliferating in the presence of $p16^{INK4A}$. However, it is important to note that the proliferation line in chordomas differs between control and induced cells. This suggests that chordoma growth is slowed by re-expression of $p16^{INK4A}$ but does not cause a state of cellular senescence. To determine whether re-expression of $p16^{INK4A}$ induces cellular senescence in PD chordomas, the standard senescence-associated acidic β-galactosidase assay was performed in PD chordomas and RTs after $p16^{INK4A}$ re-expression (Figure 3E). After 5 days of $p16^{INK4A}$ re-expression, minimal staining, approximately 4% (±0.8%), was observed for β-galactosidase in both PD chordomas. This contrasts with the RT cell lines in which 23.1% (±5%) of G401 cells and 26.3% (±7) of TTC642 stained positive for β-galactosidase. These studies indicate that the re-expression of $p16^{INK4A}$ induces cellular senescence in RT cell lines. However, PD chordomas lack sensitivity to both $p16^{INK4A}$ and SMARCB1 re-expression, as shown by minimal evidence of growth arrest and induction of cellular senescence.

Mechanisms of Gene Silencing Differ Among SWI/SNF—Mutant Cancers

Several recent reviews have implicated epigenetic inhibitors as potential treatment options for SWI/SNF mutant cancers.[14,65,66] In support of this paradigm, studies have shown that histone deacetylase (HDAC) inhibitors can lead to SMARCA2 re-expression in SMARCB1-negative RT and

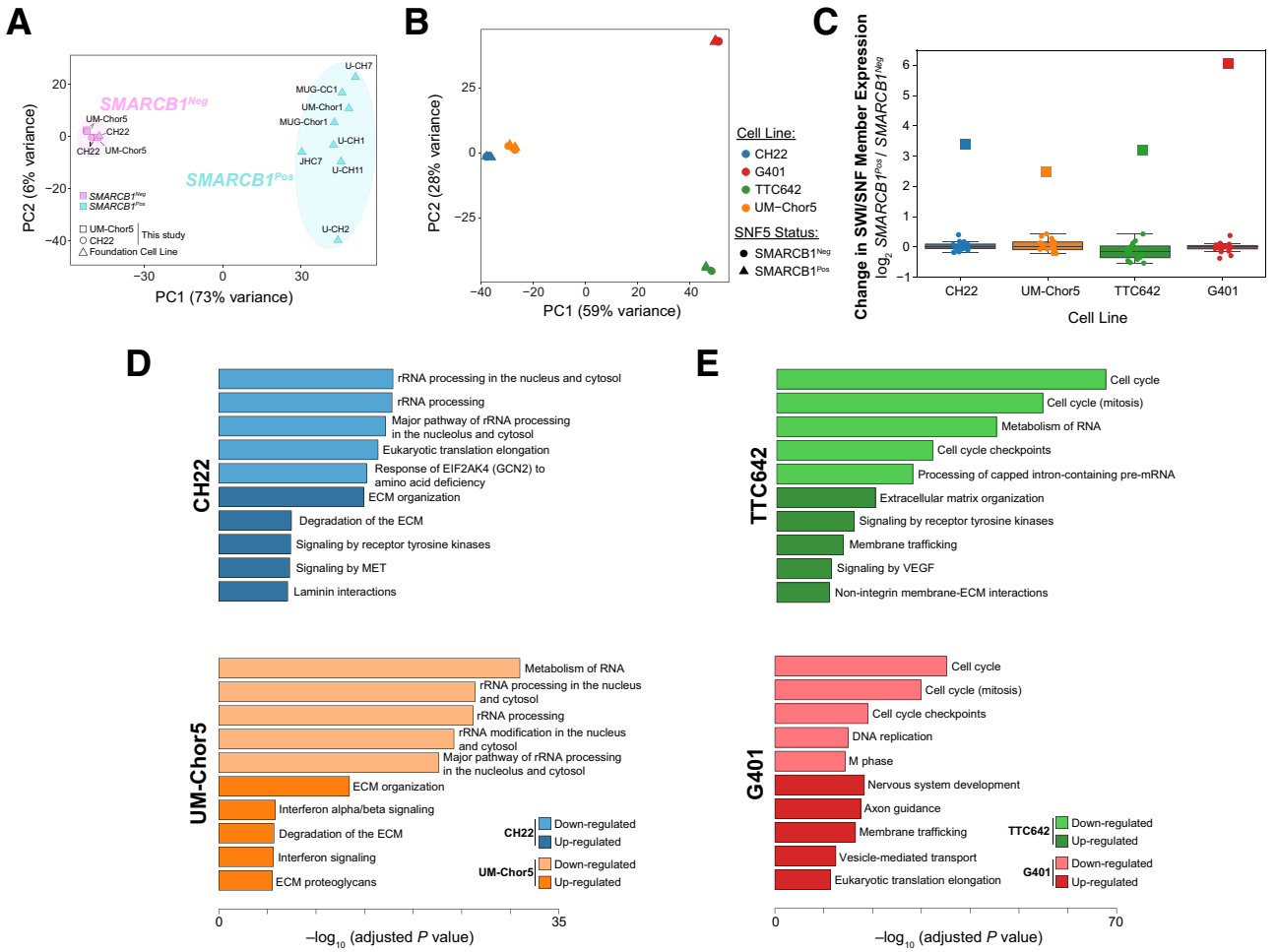

Figure 6 SMARCB1 is a major driver of gene expression with differing impacts in poorly differentiated chordomas and rhabdoid tumors. **A:** PCA plot of global gene expression between SMARCB1-inducible cell lines CH22, UM-Chor5, TTC642, and G401, as well as Chordoma Foundation samples. SMARCB1 positive (**light blue**) and SMARCB1 negative (**pink**) are represented as **triangles**, **squares**, and **circles** for Chordoma Foundation samples, SMARCB1-inducible UM-Chor5 samples, and SMARCB1-inducible CH22 samples, respectively. PC1 and PC2 are shown on these axes along with their contributions to variance. **B:** PCA plot of global gene expression between SMARCB1-inducible CH22 (**blue**), UM-Chor5 (**orange**), TTC642 (**green**), and G401 (**red**). PC1 and PC2 shown here with respective contributions to variance. SMARCB1-positive and SMARCB1-negative samples are represented as a **triangle** or **circle**. **C:** Box plot of relative $\log_2$ gene expression (transcripts per million) changes among Switch/Sucrose Non-Fermentable (SWI/SNF) complex members after re-introduction of SMARCB1. Within each cell line and each SWI/SNF complex member, the $\log_2$ fold change was calculated between average gene expression values (transcripts per million) across replicates for SMARCB1-positive and SMARCB1-negative samples, as seen on the *y* axis. The *SMARCB1* gene is represented as a **square**, and the others are represented as a **circle**. SMARCB1-inducible cell lines CH22 (**blue**), UM-Chor5 (**orange**), TTC642 (**green**), and G401 (**red**) are shown. **D:** Reactome pathways and $-\log_{10}$ adjusted *P* values calculated for differentially expressed genes in poorly differentiated chordoma cell lines CH22 (**blue**) and UM-Chor5 (**orange**). Up-regulated gene pathways are shaded darker, and down-regulated gene pathways are shaded lighter. **E:** Reactome pathways and $-\log_{10}$ adjusted *P* values calculated for differentially expressed genes in rhabdoid tumor cell lines TTC642 (**green**) and G401 (**red**). Up-regulated gene pathways are shaded darker, and down-regulated gene pathways are shaded lighter. ECM, extracellular matrix; MET, mesenchymal-epithelial transition; VEGF, vascular endothelial growth factor.

SMARCA4-negative SCCOHT cell lines consistent with epigenetic silencing.[63] Other studies have shown that enhancer of zeste homolog 2 (EZH2) inhibitors can stop proliferation of these same cell lines through induction of $p16^{INK4A}$ in the case of RT cell lines and an unknown mechanism for SCCOHT cells.[67] Because of the lack of SMARCA2 and $p16^{INK4A}$ expression in the chordoma cell lines, the effects of these epigenetic inhibitors on SMARCA2 expression were investigated.

To examine if SMARCA2 expression could be activated in PD chordomas, the SMARCB1-negative CH22 and UM-Chor5 and SMARCA4-negative COV434 cell lines were treated with either the HDAC inhibitor quisinostat (10 nmol/L) or the EZH2 inhibitor UNC1999 (10 μmol/L) for 5 days. These inhibitors were chosen based on previous reports establishing their effectiveness in reversing gene silencing in multiple human tumor cell lines, including SMARCA2/A4–deficient SCCOHT cells.[48,53,63] In addition, UNC1999, developed at the University of North Carolina at Chapel Hill, inhibits both EZH1 and EZH2. Although both HDAC and EZH1/2 inhibitors caused re-expression of SMARCA2 in the SCCOHT cell line,

SMARCA2 re-expression was not observed with either epigenetic inhibitor in the chordoma cell lines (Figure 5, A and B). The expression of another gene, *CD44*, which could be re-expressed in SMARCA4-deficient cell lines by SMARCA4 re-expression and/or HDAC inhibitors, was examined.[60,63] Although the HDAC inhibitor induced CD44 expression in the COV434 SCCOHT cell line, CD44 expression was not observed in either chordoma cell line (Figure 5A). The EZH1/2 inhibitor did not lead to CD44 re-expression in any of the cell lines. Treatment of RT and SCCOHT cell lines with these epigenetic inhibitors has also been shown to inhibit cell proliferation.[63,67,68] Therefore, whether either inhibitor affected the growth of the PD chordoma cell lines was ascertained. As shown in Figure 5C, quisinostat almost completely inhibited the growth of the COV434 cell line at 5 nmol/L, whereas the CH22 and UM-Chor5 cell lines required 50 nmol/L for a near complete growth inhibition. However, response to GSK-126 for all three cell lines appeared similar, with significant inhibition of growth at 10 μmol/L (Figure 5D). These findings implicate a different mechanism for gene silencing in SMARCB1-negative chordomas compared with other cell lines with SWI/SNF complex deficiencies.

Differential Effects on Gene Expression after Re-Expression of SMARCB1 on PD Chordoma and RT Cell Lines

To further decipher the role of SMARCB1 loss in the development of PD chordomas, differentially expressed genes after SMARCB1 re-expression were identified by RNA-sequencing. Comparisons were also made of differentially expressed genes in the PD chordomas after SMARCB1 re-expression versus those found in RT cell lines after SMARCB1 re-expression as another way to assess similarities and differences between these two SMARCB1-deficient cancers (Figure 6). To further assess the impact of SMARCB1 status in global PD chordoma gene expression, RNA-sequencing from our two SMARCB1-negative PD chordoma lines, CH22 and UM-Chor5, was compared with publicly available RNA-sequencing data from SMARCB1-positive well-differentiated chordoma lines from the Chordoma Foundation (Figure 6A). The levels of SMARCB1 expression accounted for 73% (PC1) of all RNA variance between PD and well-differentiated chordoma cell lines. Next, gene expression in the two PD chordoma cell lines with and without SMARCB1 were compared with our two RT cell lines under the same conditions. As expected, the largest scale RNA differences were driven by the cancer types; where PC1 is attributed to the variances between PD chordomas or RTs, PC2 explains the differences within RT subtypes, and PC3 describes the variance due to PD chordoma subtypes (Figure 6B and Supplemental Figure S3). However, after accounting for the differences due to cancer type, the next driving factor between samples was the presence or absence of SMARCB1 as seen in PC4 (Supplemental Figure S3). This suggests that SMARCB1 status is a driving factor in these cancers.

Gene expression of all SWI/SNF complex members was examined to ensure that the previous results were due to SMARCB1 induction alone in the DOX-inducible PD chordoma and RT cell lines (Figure 6C and Supplemental Figure 3). Induction of SMARCB1 increased levels from 4- to 64-fold (Figure 6C) but had a minimal effect on expression level changes of other SWI/SNF complex members. This suggests that the induction and re-expression of SMARCB1 was specific and is the driving variable in observed RNA-sequencing changes.

Gene expression and pathway changes that occurred after SMARCB1 induction in each cell line were identified and compared with the PD chordomas and RT samples. Interestingly, minimal overlap was observed between all four samples (178 up-regulated, 35 down-regulated). Also, the RTs had more differentially expressed genes in common with each other (594 up-regulated, 382 down-regulated) than PD chordomas had with each other (82 up-regulated, 45 down-regulated) (Supplemental Figure S3). This highlights the importance of cellular context in SMARCB1 function. Of note, all four cell lines down-regulated expression of RNA polymerase I subunit B (POLR1B) that is responsible for the transcription of rRNA. Likewise, all four cell lines shared an up-regulation of the gene *ST6GALNAC2*, which plays a role in cell−substrate interactions and protein targeting.

Pathway analyses on differentially expressed genes showed that PD chordomas and RTs have dissimilar pathway changes after SMARCB1 induction (Figure 6, D and E, and Supplemental Figure S3). Both RT cell lines had down-regulation of cell cycle pathways, consistent with the inhibition of growth observed after SMARCB1 re-expression. Decreased expression of cell cycle pathways in PD chordoma cell lines was not observed, reflecting the lack of significant growth inhibition by SMARCB1 re-expression. However, both PD chordoma cell lines showed down-regulation of pathways involved in RNA and rRNA processing. Pathways that were up-regulated after SMARCB1 re-expression presented a more complicated picture (Figure 6, D and E). PD chordoma cell lines shared up-regulation of degradation of extracellular pathways, whereas the two RT cell lines showed common up-regulation of membrane trafficking. Importantly, both PD chordoma cell lines and the TTC642 RT cell line showed the most significantly increased pathways as those regulating extracellular matrix organization. Furthermore, the CH22 PD chordoma and the TTC642 RT cell lines had significant up-regulation of signaling by receptor tyrosine receptors in common. The G401 cell line appeared to share the least in common with the other three SMARCB1-negative cell lines for up-regulated pathways (Figure 6, D and E). These results suggest that, although SMARCB1 re-expression affected expression of different genes in each PD

chordoma cell line, they converge onto similar pathways. These findings highlight the context-dependent role that SMARCB1 loss plays in cell lines from different human tumors.

Discussion

This study presents a comprehensive characterization of SMARCB1-negative PD chordomas with an emphasis on understanding how its loss may drive development of these clinically aggressive tumors. Overall, the results show that SMARCB1 loss plays a relatively unique role in the etiology of PD chordomas compared with the more extensively characterized SMARCB1-negative RTs. Although re-expression of SMARCB1 in deficient RT cell lines caused a rapid inhibition of cell growth followed by the induction of replicative senescence, its re-expression in PD chordoma cell lines showed little effect on cellular proliferation. Thus, these results imply that SMARCB1 loss contributes to PD chordoma development in a fundamentally different way from its role in RT etiology.

Multiple studies have linked the growth arrest and cellular senescence induced by SMARCB1 re-expression in RT cell lines to $p16^{INK4A}$ re-expression through eviction of the PRC2 complex from its promoter.[25,26] Loss of SMARCB1 affecting proliferation has been reported in other SMARCB1-deficient cell lines, including renal medullary carcinomas, although the role of $p16^{INK4A}$ re-expression was not discussed.[69] However, the majority of chordomas, regardless of SMARCB1 status, have genetic inactivation of the *CDKN2* (*$p16^{INK4A}$*) gene, rendering them incapable of its normal expression. Both SMARCB1-negative PD chordoma cell lines have deletions of $p16^{INK4A}$ and lack its expression (Figure 4A). However, unlike RT cell lines, $p16^{INK4A}$ expression did not cause growth arrest and cellular senescence in both PD chordoma cell lines, consistent with a dysfunctional Rb pathway. This result resembles those of previous publications showing that re-expression of $p16^{INK4A}$ in SMARCA4-deficient lung, breast, and other carcinoma cell lines failed to induce growth arrest without concomitant re-expression of SMARCA4.[70–73] Thus, $p16^{INK4A}$-induced growth arrest in PD chordoma cell lines may require re-expression of SMARCB1. The role of $p16^{INK4A}$ in SMARCB1-induced growth arrest seems consistent with previous reports in other SMARCB1-deficient tumor cell lines. Growth arrest occurred in renal medullary carcinoma cells after SMARCB1 re-expression, another tumor that retains a wild-type *$p16^{INK4A}$* gene.[74] In contrast, Nakayama et al[51] reported that SMARCB1 re-expression in three out of four human SMARCB1-negative epithelioid sarcoma cell lines did not induce growth arrest, another tumor in which 38% of primary tumors lack $p16^{INK4A}$ expression.

Both SMARCB1-negative PD chordoma and RT cell lines lack expression of SMARCA2, the mutually exclusive ATPase from SMARCA4 in SWI/SNF complexes. Loss of SMARCA2 expression by epigenetic silencing frequently occurs in primary tumors and cell lines with inactivating mutations of *SMARCA4* or *SMARCB1* such as RTs, SCCOHT, and lung adenocarcinoma.[54,75,76] Consistent with the paradigm, the PD chordoma cell lines did not express SMARCA2 protein (Figure 1, A and B). Surprisingly, primary PD chordomas retained robust expression of SMARCA2 by IHC (Figure 2 and Supplemental Figure S2). Thus, the current results implicate SMARCA2 loss as part of the process of establishing PD chordoma cell lines in cell culture. However, the possibility of selection for growth in culture of a rare population of SMARCA2-negative PD chordoma cells cannot be ruled out. The mechanism by which loss of SMARCA2 expression occurs during this process may also differ from the epigenetic silencing observed in primary tumors. Although the current results replicated previous studies with SMARCA2 re-expression in SCCOHT cell lines after treatment with HDACs and EZH2 inhibitors, the agents did not induce SMARCA2 re-expression in PD chordomas. This result suggests that SMARCA2 is not epigenetically silenced in PD chordomas or that more robust epigenetic inhibitor screens are needed. These findings also indicate that additional SWI/SNF complex members should be investigated as therapeutic targets in PD chordoma (eg, BRD9 and BAF180).[6,64]

Next-generation sequencing has revealed that more than 50% of human cancers harbor mutations in enzymes involved in chromatin organization.[12] Tumor cells are not only activated by genetic and epigenetic alterations but also routinely use epigenetic processes to ensure their escape from chemotherapy and host immune surveillance. Hence, a growing emphasis of recent drug discovery efforts has been on targeting the epigenome.[63,77–79] Alternatively, the development of small molecules to target SWI/SNF complex members may provide novel treatment strategies for PD chordomas and other SWI/SNF−mutant cancers.[65,66] However, SMARCB1 protein may prove an undruggable target because it plays a critical role in genomic transcriptional control. The Gene Ontology analysis of the gene expression changes for SMARCB1 re-expression in the PD chordoma cell lines identified down-regulation of rRNA pathways. This finding suggests that targeting the disruption of the ribosome translational machinery may provide novel therapeutic targets.[80] Additional investigation is necessary to evaluate these subunits and drug classes as potential therapeutic options in PD chordomas.

The current results support a model in which SMARCB1 loss plays different roles in the initiation or progression of tumorigenesis among SWI/SNF−mutant cancers. As a core component of human BAF and PBAF SWI/SNF complexes, loss of SMARCB1 profoundly alters SWI/SNF complex functions and/or specificity.[49–51] If SMARCB1 loss caused similar chromatin changes across all cancers, we would expect to observe similar patterns of gene expression changes after SMARCB1 re-expression. However, we saw

significantly different gene expression alterations after SMARCB1 re-expression between the RT and PD chordoma cell lines. In RT cell lines, SMARCB1 re-expression caused changes in RNA expression of approximately 10 times more genes. In addition, enrichment was observed for down-regulation of cell cycle pathways after SMARCB1 re-expression, consistent with induction of growth arrest in culture. In contrast, our analysis of the RNA-sequencing data identified an up-regulation of pathways involved in development after SMARCB1 re-expression in PD chordomas, supporting a role for SMARCB1 loss in driving the PD phenotype of these cancers.

We propose that SMARCB1 loss acts as the singular initiation event in the development of RTs, in the absence of additional, consistent mutations in these cancers.[24,81–83] In contrast, studies on chordoma biology and histopathology suggest that PD chordomas develop from a well-differentiated tumor, presumably after inactivation of the *SMARCB1* gene.[84] Thus, unlike RTs, PD chordomas possess mutations in other classic oncogenes and tumor suppressor genes such as *CDKN2A*, *TP53*, and *EGFR*.[6,64] Our SMARCB1 re-expression studies in PD chordoma and RT cell lines further support this model in which we observed increased expression of differentiation genes in the PD chordoma cell lines and up-regulation of cell cycle regulatory genes in RT cell lines. Consistent with this notion, a study by Vitte et al[85] showed that early SMARCB1 loss causes RTs whereas loss at later stages combined with *NF2* gene inactivation causes schwannomas. As with many SWI/SNF complex members, SMARCB1 seems to manifest its tumor suppressor functions through changes in gene expression and chromatin accessibility.[50,51] Therefore, the mechanisms by which SMARCB1 loss contributes to the initiation of RTs and to the progression of PD chordomas may involve binding of SWI/SNF complexes to different sites in the genome. Future epigenomic studies determining changes in global SMARCB1 binding and chromatin accessibility experiments should identify additional unique and common binding sites for SWI/SNF complex members to address this model.

Acknowledgments

We thank Rayvon Martin and David Alcorta, Ph.D., for technical support.

Supplemental Data

Supplemental material for this article can be found at *http://doi.org/10.1016/j.ajpath.2022.12.012*.

References

1. Beccaria K, Sainte-Rose C, Zerah M, Puget S: Paediatric chordomas. Orphanet J Rare Dis 2015, 10:116
2. Habrand J-L, Datchary J, Bolle S, Beaudré A, de Marzi L, Beccaria K, Stefan D, Grill J, Dendale R: Chordoma in children: case-report and review of literature. Rep Pract Oncol Radiother 2016, 21: 1–7
3. Hoch BL, Nielsen GP, Liebsch NJ, Rosenberg AE: Base of skull chordomas in children and adolescents: a clinicopathologic study of 73 cases. Am J Surg Pathol 2006, 30:811–818
4. Walcott BP, Nahed BV, Mohyeldin A, Coumans J-V, Kahle KT, Ferreira MJ: Chordoma: current concepts, management, and future directions. Lancet Oncol 2012, 13:e69–e76
5. Choy E, MacConaill LE, Cote GM, Le LP, Shen JK, Nielsen GP, Iafrate AJ, Garraway LA, Hornicek FJ, Duan Z: Genotyping cancer-associated genes in chordoma identifies mutations in oncogenes and areas of chromosomal loss involving CDKN2A, PTEN, and SMARCB1. PLoS One 2014, 9:e101283
6. Tarpey PS, Behjati S, Young MD, Martincorena I, Alexandrov LB, Farndon SJ, Guzzo C, Hardy C, Latimer C, Butler AP, Teague JW, Shlien A, Futreal PA, Shah S, Bashashati A, Jamshidi F, Nielsen TO, Huntsman D, Baumhoer D, Brandner S, Wunder J, Dickson B, Cogswell P, Sommer J, Phillips JJ, Amary MF, Tirabosco R, Pillay N, Yip S, Stratton MR, Flanagan AM, Campbell PJ: The driver landscape of sporadic chordoma. Nat Commun 2017, 8:890
7. Vanderheijden C, Vaessen T, Yakkioui Y, Temel Y, Hoogland G, Hovinga K: Genes predicting survival of chordoma patients. World Neurosurg 2021, 156:125–132
8. Zuckerman SL, Bilsky MH, Laufer I: Chordomas of the skull base, mobile spine, and sacrum: an epidemiologic investigation of presentation, treatment, and survival. World Neurosurg 2018, 113: e618–e627
9. Bakker SH, Jacobs WCH, Pondaag W, Gelderblom H, Nout RA, Dijkstra PDS, Peul WC, Vleggeert-Lankamp CLA: Chordoma: a systematic review of the epidemiology and clinical prognostic factors predicting progression-free and overall survival. Eur Spine J 2018, 27:3043–3058
10. Smoll NR, Gautschi OP, Radovanovic I, Schaller K, Weber DC: Incidence and relative survival of chordomas: the standardized mortality ratio and the impact of chordomas on a population. Cancer 2013, 119:2029–2037
11. Cha YJ, Hong C-K, Kim D-S, Lee S-K, Park HJ, Kim SH: Poorly differentiated chordoma with loss of SMARCB1/INI1 expression in pediatric patients: a report of two cases and review of the literature. Neuropathology 2018, 38:47–53
12. Kadoch C, Hargreaves DC, Hodges C, Elias L, Ho L, Ranish J, Crabtree GR: Proteomic and bioinformatic analysis of mammalian SWI/SNF complexes identifies extensive roles in human malignancy. Nat Genet 2013, 45:592–601
13. Michel BC, D'Avino AR, Cassel SH, Mashtalir N, McKenzie ZM, McBride MJ, Valencia AM, Zhou Q, Bocker M, Soares LMM, Pan J, Remillard DI, Lareau CA, Zullow HJ, Fortoul N, Gray NS, Bradner JE, Chan HM, Kadoch C: A non-canonical SWI/SNF complex is a synthetic lethal target in cancers driven by BAF complex perturbation. Nat Cell Biol 2018, 20:1410–1420
14. Orlando KA, Nguyen V, Raab JR, Walhart T, Weissman BE: Remodeling the cancer epigenome: mutations in the SWI/SNF complex offer new therapeutic opportunities. Expert Rev Anticancer Ther 2019, 19:375–391
15. Biegel JA, Fogelgren B, Wainwright LM, Zhou JY, Bevan H, Rorke LB: Germline INI1 mutation in a patient with a central nervous system atypical teratoid tumor and renal rhabdoid tumor. Genes Chromosomes Cancer 2000, 28:31–37
16. Versteege I, Sevenet N, Lange J, Rousseau-Merck MF, Ambros P, Handgretinger R, Aurias A, Delattre O: Truncating mutations of hSNF5/INI1 in aggressive paediatric cancer. Nature 1998, 394: 203–206
17. Modena P, Lualdi E, Facchinetti F, Galli L, Teixeira MR, Pilotti S, Sozzi G: SMARCB1/INI1 tumor suppressor gene is frequently inactivated in epithelioid sarcomas. Cancer Res 2005, 65:4012–4019

18. Calderaro J, Moroch J, Pierron G, Pedeutour F, Grison C, Maillé P, Soyeux P, de la Taille A, Couturier J, Vieillefond A, Rousselet MC, Delattre O, Allory Y: SMARCB1/INI1 inactivation in renal medullary carcinoma. Histopathology 2012, 61:428−435
19. Parker NA, Al-Obaidi A, Deutsch JM: SMARCB1/INI1-deficient tumors of adulthood. F1000Res 2020, 9:662
20. Sirohi DM, Ohe C, Smith SC, Amin MB: SWI/SNF-deficient neoplasms of the genitourinary tract. Semin Diagn Pathol 2021, 38: 212−221
21. Hui Y, Cotzia P, Rana S, Kezlarian BE, Lin O, Hollmann TJ, Dogan S: Primary cutaneous SMARCB1-deficient carcinoma. J Cutan Pathol 2021, 48:1051−1060
22. Forrest SJ, Al-Ibraheemi A, Doan D, Ward A, Clinton CM, Putra J, Pinches RS, Kadoch C, Chi SN, DuBois SG, Leavey PJ, LeBoeuf NR, Mullen E, Collins N, Church AJ, Janeway KA: Genomic and immunologic characterization of INI1-deficient pediatric cancers. Clin Cancer Res 2020, 26:2882−2890
23. Hasselblatt M, Isken S, Linge A, Eikmeier K, Jeibmann A, Oyen F, Nagel I, Richter J, Bartelheim K, Kordes U, Schneppenheim R, Frühwald M, Siebert R, Paulus W: High-resolution genomic analysis suggests the absence of recurrent genomic alterations other than SMARCB1 aberrations in atypical teratoid/rhabdoid tumors. Genes Chromosomes Cancer 2013, 52:185−190
24. Lee RS, Stewart C, Carter SL, Ambrogio L, Cibulskis K, Sougnez C, Lawrence MS, Auclair D, Mora J, Golub TR, Biegel JA, Getz G, Roberts CWM: A remarkably simple genome underlies highly malignant pediatric rhabdoid cancers. J Clin Invest 2012, 122: 2983−2988
25. Kia SK, Gorski MM, Giannakopoulos S, Verrijzer CP: SWI/SNF mediates polycomb eviction and epigenetic reprogramming of the INK4b-ARF-INK4a locus. Mol Cell Biol 2008, 28:3457−3464
26. Wilson BG, Wang X, Shen X, McKenna ES, Lemieux ME, Cho Y-J, Koellhoffer EC, Pomeroy SL, Orkin SH, Roberts CWM: Epigenetic antagonism between polycomb and SWI/SNF complexes during oncogenic transformation. Cancer Cell 2010, 18:316−328
27. von Witzleben A, Goerttler LT, Marienfeld R, Barth H, Lechel A, Mellert K, Böhm M, Kornmann M, Mayer-Steinacker R, von Baer A, Schultheiss M, Flanagan AM, Möller P, Brüderlein S, Barth TFE: Preclinical characterization of novel chordoma cell systems and their targeting by pharmacological inhibitors of the CDK4/6 cell-cycle pathway. Cancer Res 2015, 75:3823−3831
28. Dowdy SF, Fasching CL, Araujo D, Lai KM, Livanos E, Weissman BE, Stanbridge EJ: Suppression of tumorigenicity in Wilms tumor by the p14:p15 region of chromosome 11. Science 1991, 254:293−295
29. Weissman BE, Saxon PJ, Pasquale SR, Jones GR, Geiser AG, Stanbridge EJ: Introduction of a normal human chromosome 11 into a Wilms' tumor cell line controls its tumorigenic expression. Science 1987, 236:175−180
30. Weissman BE, Stanbridge EJ: Characterization of ouabain-resistant, hypoxanthine guanine phosphoribosyl transferase deficient human cells and their usefulness as a general method for the production of human cell hybrids. Cytogenet Cell Genet 1980, 28:227−239
31. Ramos P, Karnezis AN, Craig DW, Sekulic A, Russell ML, Hendricks WPD, Corneveaux JJ, Barrett MT, Shumansky K, Yang Y, Shah SP, Prentice LM, Marra MA, Kiefer J, Zismann VL, McEachron TA, Salhia B, Prat J, D'Angelo E, Clarke BA, Pressey JG, Farley JH, Anthony SP, Roden RBS, Cunliffe HE, Huntsman DG, Trent JM: Small cell carcinoma of the ovary, hypercalcemic type, displays frequent inactivating germline and somatic mutations in SMARCA4. Nat Genet 2014, 46:427−429
32. Karnezis AN, Chen SY, Chow C, Yang W, Hendricks WPD, Ramos P, Briones N, Mes-Masson A-M, Bosse T, Gilks CB, Trent JM, Weissman B, Huntsman DG, Wang Y: Re-assigning the histologic identities of COV434 and TOV-112D ovarian cancer cell lines. Gynecol Oncol 2021, 160:568−578
33. Wei D, Goldfarb D, Song S, Cannon C, Yan F, Sakellariou-Thompson D, Emanuele M, Major MB, Weissman BE, Kuwahara Y: SNF5/INI1 deficiency redefines chromatin remodeling complex composition during tumor development. Mol Cancer Res 2014, 12: 1574−1585
34. Howard TP, Arnoff TE, Song MR, Giacomelli AO, Wang X, Hong AL, Dharia NV, Wang S, Vazquez F, Pham M-T, Morgan AM, Wachter F, Bird GH, Kugener G, Oberlick EM, Rees MG, Tiv HL, Hwang JH, Walsh KH, Cook A, Krill-Burger JM, Tsherniak A, Gokhale PC, Park PJ, Stegmaier K, Walensky LD, Hahn WC, Roberts CWM: MDM2 and MDM4 are therapeutic vulnerabilities in malignant rhabdoid tumors. Cancer Res 2019, 79:2404−2414
35. Lorzadeh A, Hammond C, Wang F, Knapp DJHF, Wong JC, Zhu JYA, Cao Q, Heravi-Moussavi A, Carles A, Wong M, Sharafian Z, Steif J, Moksa M, Bilenky M, Lavoie PM, Eaves CJ, Hirst M: Polycomb contraction differentially regulates terminal human hematopoietic differentiation programs. BMC Biol 2022, 20:104
36. Martin M: Cutadapt removes adapter sequences from high-throughput sequencing reads. EMBnet J 2011, 17:10−12
37. Dobin A, Davis CA, Schlesinger F, Drenkow J, Zaleski C, Jha S, Batut P, Chaisson M, Gingeras TR: STAR: ultrafast universal RNA-seq aligner. Bioinformatics 2013, 29:15−21
38. Noda M, Sato SA, Hirokawa Y, Uemoto M, Takeuchi T, Yamada S, Yamada A, Shinohara Y, Yamaguchi M, Iida K, Floss I, Otobe T, Lee K-M, Ishimura K, Boku T, Bertsch GF, Nobusada K, Yabana K: SALMON: Scalable Ab-initio Light−Matter simulator for optics and nanoscience. Comput Phys Commun 2019, 235:356−365
39. Li H, Handsaker B, Wysoker A, Fennell T, Ruan J, Homer N, Marth G, Abecasis G, Durbin R; 1000 Genome Project Data Processing Subgroup: The sequence alignment/map format and SAMtools. Bioinformatics 2009, 25:2078−2079
40. Quinlan AR, Hall IM: BEDTools: a flexible suite of utilities for comparing genomic features. Bioinformatics 2010, 26:841−842
41. Hunter JD: Matplotlib: a 2D graphics environment. Comput Sci Eng 2007, 9:90−95
42. R Core Team: R: A Language and Environment for Statistical Computing. Vienna, Austria, R Foundation for Statistical Computing, 2012
43. Love MI, Huber W, Anders S: Moderated estimation of fold change and dispersion for RNA-seq data with DESeq2. Genome Biol 2014, 15:550
44. Gillespie M, Jassal B, Stephan R, Milacic M, Rothfels K, Senff-Ribeiro A, Griss J, Sevilla C, Matthews L, Gong C, Deng C, Varusai T, Ragueneau E, Haider Y, May B, Shamovsky V, Weiser J, Brunson T, Sanati N, Beckman L, Shao X, Fabregat A, Sidiropoulos K, Murillo J, Viteri G, Cook J, Shorser S, Bader G, Demir E, Sander C, Haw R, Wu G, Stein L, Hermjakob H, D'Eustachio P: The reactome pathway knowledgebase 2022. Nucleic Acids Res 2022, 50:D687−D692
45. Raudvere U, Kolberg L, Kuzmin I, Arak T, Adler P, Peterson H, Vilo J: g:Profiler: a web server for functional enrichment analysis and conversions of gene lists (2019 update). Nucleic Acids Res 2019, 47: W191−W198
46. Waskom ML: seaborn: statistical data visualization. J Open Source Softw 2021, 6:3021
47. Conway JR, Lex A, Gehlenborg N: UpSetR: an R package for the visualization of intersecting sets and their properties. Bioinformatics 2017, 33:2938−2940
48. Karnezis AN, Wang Y, Ramos P, Hendricks WP, Oliva E, D'Angelo E, Prat J, Nucci MR, Nielsen TO, Chow C, Leung S, Kommoss F, Kommoss S, Silva A, Ronnett BM, Rabban JT, Bowtell DD, Weissman BE, Trent JM, Gilks CB, Huntsman DG: Dual loss of the SWI/SNF complex ATPases SMARCA4/BRG1 and SMARCA2/BRM is highly sensitive and specific for small cell carcinoma of the ovary, hypercalcaemic type. J Pathol 2016, 238: 389−400

49. Mashtalir N, D'Avino AR, Michel BC, Luo J, Pan J, Otto JE, Zullow HJ, McKenzie ZM, Kubiak RL, St. Pierre R, Valencia AM, Poynter SJ, Cassel SH, Ranish JA, Kadoch C: Modular organization and assembly of SWI/SNF family chromatin remodeling complexes. Cell 2018, 175:1272−1288.e20
50. Wang X, Lee RS, Alver BH, Haswell JR, Wang S, Mieczkowski J, Drier Y, Gillespie SM, Archer TC, Wu JN, Tzvetkov EP, Troisi EC, Pomeroy SL, Biegel JA, Tolstorukov MY, Bernstein BE, Park PJ, Roberts CWM: SMARCB1-mediated SWI/SNF complex function is essential for enhancer regulation. Nat Genet 2017, 49:289−295
51. Nakayama RT, Pulice JL, Valencia AM, McBride MJ, McKenzie ZM, Gillespie MA, Ku WL, Teng M, Cui K, Williams RT, Cassel SH, Qing H, Widmer CJ, Demetri GD, Irizarry RA, Zhao K, Ranish JA, Kadoch C: SMARCB1 is required for widespread BAF complex-mediated activation of enhancers and bivalent promoters. Nat Genet 2017, 49:1613−1623
52. DeCristofaro MF, Betz BL, Rorie CJ, Reisman DN, Wang W, Weissman BE: Characterization of SWI/SNF protein expression in human breast cancer cell lines and other malignancies. J Cell Physiol 2001, 186:136−145
53. Yamamichi N, Yamamichi-Nishina M, Mizutani T, Watanabe H, Minoguchi S, Kobayashi N, Kimura S, Ito T, Yahagi N, Ichinose M, Omata M, Iba H: The Brm gene suppressed at the post-transcriptional level in various human cell lines is inducible by transient HDAC inhibitor treatment, which exhibits antioncogenic potential. Oncogene 2005, 24:5471−5481
54. Glaros S, Cirrincione GM, Muchardt C, Kleer CG, Michael CW, Reisman D: The reversible epigenetic silencing of BRM: implications for clinical targeted therapy. Oncogene 2007, 26:7058−7066
55. Biegel JA, Zhou JY, Rorke LB, Stenstrom C, Wainwright LM, Fogelgren B: Germ-line and acquired mutations of INI1 in atypical teratoid and rhabdoid tumors. Cancer Res 1999, 59:74−79
56. Biegel JA, Tan L, Zhang F, Wainwright L, Russo P, Rorke LB: Alterations of the hSNF5/INI1 gene in central nervous system atypical teratoid/rhabdoid tumors and renal and extrarenal rhabdoid tumors. Clin Cancer Res 2002, 8:3461−3467
57. Judkins AR, Mauger J, Ht A, Rorke LB, Biegel JA: Immunohistochemical analysis of hSNF5/INI1 in pediatric CNS neoplasms. Am J Surg Pathol 2004, 28:644−650
58. Betz BL, Strobeck MW, Reisman DN, Knudsen ES, Weissman BE: Re-expression of hSNF5/INI1/BAF47 in pediatric tumor cells leads to G1 arrest associated with induction of p16ink4a and activation of RB. Oncogene 2002, 21:5193−5203
59. Versteege I, Medjkane S, Rouillard D, Delattre O: A key role of the hSNF5/INI1 tumour suppressor in the control of the G1-S transition of the cell cycle. Oncogene 2002, 21:6403−6412
60. Strobeck MW, DeCristofaro MF, Banine F, Weissman BE, Sherman LS, Knudsen ES: The BRG-1 subunit of the SWI/SNF complex regulates CD44 expression. J Biol Chem 2001, 276: 9273−9278
61. Senbanjo LT, Chellaiah MA: CD44: a multifunctional cell surface adhesion receptor is a regulator of progression and metastasis of cancer cells. Front Cell Dev Biol 2017, 5:18
62. Sneath RJ, Mangham DC: The normal structure and function of CD44 and its role in neoplasia. Mol Pathol 1998, 51:191−200
63. Wang Y, Chen SY, Colborne S, Lambert G, Shin CY, Santos ND, Orlando KA, Lang JD, Hendricks WPD, Bally MB, Karnezis AN, Hass R, Underhill TM, Morin GB, Trent JM, Weissman BE, Huntsman DG: Histone deacetylase inhibitors synergize with catalytic inhibitors of EZH2 to exhibit antitumor activity in small cell carcinoma of the ovary, hypercalcemic type. Mol Cancer Ther 2018, 17:2767−2779
64. Bai J, Shi J, Li C, Wang S, Zhang T, Hua X, Zhu B, Koka H, Wu H-H, Song L, Wang D, Wang M, Zhou W, Ballew BJ, Zhu B, Hicks B, Mirabello L, Parry DM, Zhai Y, Li M, Du J, Wang J, Zhang S, Liu Q, Zhao P, Gui S, Goldstein AM, Zhang Y, Yang XR: Whole genome sequencing of skull-base chordoma reveals genomic alterations associated with recurrence and chordoma-specific survival. Nat Commun 2021, 12:757
65. Valencia AM, Kadoch C: Chromatin regulatory mechanisms and therapeutic opportunities in cancer. Nat Cell Biol 2019, 21: 152−161
66. Mittal P, Roberts CWM: The SWI/SNF complex in cancer—biology, biomarkers and therapy. Nat Rev Clin Oncol 2020, 17:435−448
67. Wang Y, Chen SY, Karnezis AN, Colborne S, Santos ND, Lang JD, Hendricks WP, Orlando KA, Yap D, Kommoss F, Bally MB, Morin GB, Trent JM, Weissman BE, Huntsman DG: The histone methyltransferase EZH2 is a therapeutic target in small cell carcinoma of the ovary, hypercalcaemic type. J Pathol 2017, 242:371−383
68. Kim KH, Roberts CWM: Targeting EZH2 in cancer. Nat Med 2016, 22:128−134
69. Hong AL, Tseng Y-Y, Wala JA, Kim W-J, Kynnap BD, Doshi MB, et al: Renal medullary carcinomas depend upon SMARCB1 loss and are sensitive to proteasome inhibition. Elife 2019, 8:e44161
70. Strobeck MW, Knudsen KE, Fribourg AF, DeCristofaro MF, Weissman BE, Imbalzano AN, Knudsen ES: BRG-1 is required for RB-mediated cell cycle arrest. Proc Natl Acad Sci U S A 2000, 97: 7748−7753
71. Reisman DN, Strobeck MW, Betz BL, Sciariotta J, Funkhouser W Jr, Murchardt C, Yaniv M, Sherman LS, Knudsen ES, Weissman BE: Concomitant down-regulation of BRM and BRG1 in human tumor cell lines: differential effects on RB-mediated growth arrest vs CD44 expression. Oncogene 2002, 21:1196−1207
72. Strobeck MW, Reisman DN, Gunawardena RW, Betz BL, Angus SP, Knudsen KE, Kowalik TF, Weissman BE, Knudsen ES: Compensation of BRG-1 function by Brm: insight into the role of the core SWI-SNF subunits in retinoblastoma tumor suppressor signaling. J Biol Chem 2002, 277:4782−4789
73. Zhang HS, Gavin M, Dahiya A, Postigo AA, Ma D, Luo RX, Harbour JW, Dean DC: Exit from G1 and S phase of the cell cycle is regulated by repressor complexes containing HDAC-Rb-hSWI/SNF and Rb-hSWI/SNF. Cell 2000, 101:79−89
74. Msaouel P, Malouf GG, Su X, Yao H, Tripathi DN, Soeung M, et al: Comprehensive molecular characterization identifies distinct genomic and immune hallmarks of renal medullary carcinoma. Cancer Cell 2020, 37:720−734.e13
75. Kahali B, Yu J, Marquez SB, Thompson KW, Liang SY, Lu L, Reisman D: The silencing of the SWI/SNF subunit and anticancer gene BRM in rhabdoid tumors. Oncotarget 2014, 5:3316−3332
76. Hoffman GR, Rahal R, Buxton F, Xiang K, McAllister G, Frias E, Bagdasarian L, Huber J, Lindeman A, Chen D, Romero R, Ramadan N, Phadke T, Haas K, Jaskelioff M, Wilson BG, Meyer MJ, Saenz-Vash V, Zhai H, Myer VE, Porter JA, Keen N, McLaughlin ME, Mickanin C, Roberts CWM, Stegmeier F, Jagani Z: Functional epigenetics approach identifies BRM/SMARCA2 as a critical synthetic lethal target in BRG1-deficient cancers. Proc Natl Acad Sci U S A 2014, 111:3128−3133
77. Zhang H, Pandey S, Travers M, Sun H, Morton G, Madzo J, Chung W, Khowsathit J, Perez-Leal O, Barrero CA, Merali C, Okamoto Y, Sato T, Pan J, Garriga J, Bhanu NV, Simithy J, Patel B, Huang J, Raynal NJ-M, Garcia BA, Jacobson MA, Kadoch C, Merali S, Zhang Y, Childers W, Abou-Gharbia M, Karanicolas J, Baylin SB, Zahnow CA, Jelinek J, Graña X, Issa J-PJ: Targeting CDK9 reactivates epigenetically silenced genes in cancer. Cell 2018, 175:1244−1258.e26
78. Wang X, Wang S, Troisi EC, Howard TP, Haswell JR, Wolf BK, Hawk WH, Ramos P, Oberlick EM, Tzvetkov EP, Ross A, Vazquez F, Hahn WC, Park PJ, Roberts CWM: BRD9 defines a SWI/SNF sub-complex and constitutes a specific vulnerability in malignant rhabdoid tumors. Nat Commun 2019, 10:1881
79. Oike T, Ogiwara H, Tominaga Y, Ito K, Ando O, Tsuta K, Mizukami T, Shimada Y, Isomura H, Komachi M, Furuta K, Watanabe S-I, Nakano T, Yokota J, Kohno T: A synthetic lethality−based strategy to treat cancers harboring a genetic

deficiency in the chromatin remodeling factor BRG1. Cancer Res 2013, 73:5508–5518
80. Janin M, Coll-SanMartin L, Esteller M: Disruption of the RNA modifications that target the ribosome translation machinery in human cancer. Mol Cancer 2020, 19:70
81. McKenna ES, Sansam CG, Cho Y-J, Greulich H, Evans JA, Thom CS, Moreau LA, Biegel JA, Pomeroy SL, Roberts CWM: Loss of the epigenetic tumor suppressor SNF5 leads to cancer without genomic instability. Mol Cell Biol 2008, 28:6223–6233
82. Johann PD, Erkek S, Zapatka M, Kerl K, Buchhalter I, Hovestadt V, et al: Atypical teratoid/rhabdoid tumors are comprised of three epigenetic subgroups with distinct enhancer landscapes. Cancer Cell 2016, 29:379–393
83. Chun H-JE, Lim EL, Heravi-Moussavi A, Saberi S, Mungall KL, Bilenky M, Carles A, Tse K, Shlafman I, Zhu K, Qian JQ, Palmquist DL, He A, Long W, Goya R, Ng M, LeBlanc VG, Pleasance E, Thiessen N, Wong T, Chuah E, Zhao Y-J, Schein JE, Gerhard DS, Taylor MD, Mungall AJ, Moore RA, Ma Y, Jones SJM, Perlman EJ, Hirst M, Marra MA: Genome-wide profiles of extracranial malignant rhabdoid tumors reveal heterogeneity and dysregulated developmental pathways. Cancer Cell 2016, 29:394–406
84. Hasselblatt M, Thomas C, Hovestadt V, Schrimpf D, Johann P, Bens S, Oyen F, Peetz-Dienhart S, Crede Y, Wefers A, Vogel H, Riemenschneider MJ, Antonelli M, Giangaspero F, Bernardo MC, Giannini C, Ud Din N, Perry A, Keyvani K, van Landeghem F, Sumerauer D, Hauser P, Capper D, Korshunov A, Jones DTW, Pfister SM, Schneppenheim R, Siebert R, Frühwald MC, Kool M: Poorly differentiated chordoma with SMARCB1/INI1 loss: a distinct molecular entity with dismal prognosis. Acta Neuropathol 2016, 132:149–151
85. Vitte J, Gao F, Coppola G, Judkins AR, Giovannini M: Timing of Smarcb1 and Nf2 inactivation determines schwannoma versus rhabdoid tumor development. Nat Commun 2017, 8:300